iScience

CellPress
OPEN ACCESS

Article

Regulated adipose tissue-specific expression of human *AGPAT2* in lipodystrophic *Agpat2*-null mice results in regeneration of adipose tissue

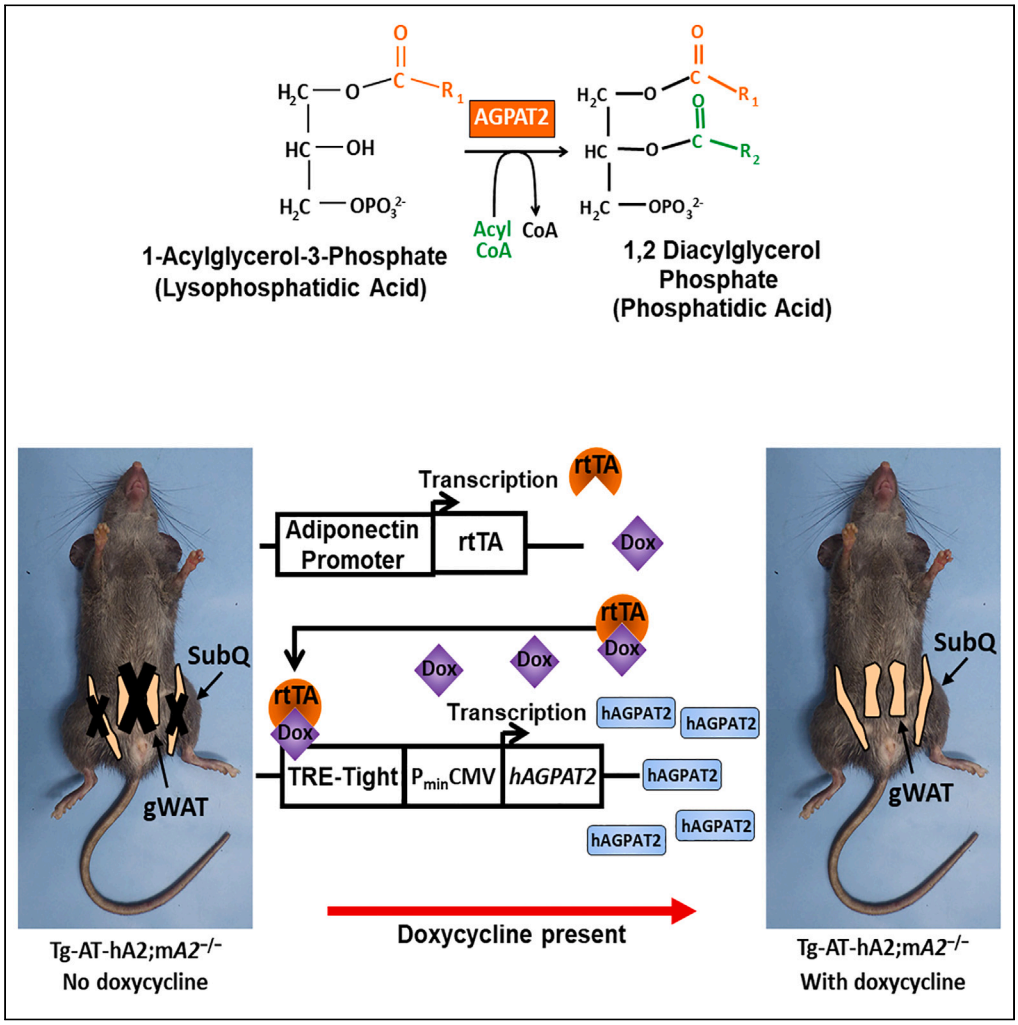

Anil K. Agarwal, Katie Tunison, Goncalo Vale, ..., Philipp E. Scherer, Jay D. Horton, Abhimanyu Garg

anil.agarwal@utsouthwestern.edu

Highlights

Re-expression of human AGPAT2 in *Agpat2*-null mice regenerates adipose tissue

Tg-$^{AT\text{-}hA2}$;mA2$^{-/-}$ mice have increased plasma leptin levels

Ex vivo SVF cells only differentiate in the presence of doxycycline

Removal of doxycycline in whole animal reduces fat pads to undetectable levels

Agarwal et al., iScience *26*, 107806
October 20, 2023 © 2023 The Author(s).
https://doi.org/10.1016/j.isci.2023.107806

iScience

CellPress
OPEN ACCESS

Article

Regulated adipose tissue-specific expression of human *AGPAT2* in lipodystrophic *Agpat2*-null mice results in regeneration of adipose tissue

Anil K. Agarwal,[1,2,6,*] Katie Tunison,[1,2] Goncalo Vale,[2,3] Jeffrey G. McDonald,[2,3] Xilong Li,[4] Philipp E. Scherer,[5] Jay D. Horton,[2,3] and Abhimanyu Garg[1,2]

SUMMARY

Genetic loss of *Agpat2* in humans and mice results in congenital generalized lipodystrophy with near-total loss of adipose tissue and predisposition to develop insulin resistance, diabetes mellitus, hepatic steatosis, and hypertriglyceridemia. The mechanism by which *Agpat2* deficiency results in loss of adipose tissue remains unknown. We studied this by re-expressing human *AGPAT2* (hAGPAT2) in *Agpat2*-null mice, regulated by doxycycline. In both sexes of *Agpat2*-null mice, adipose-tissue-specific re-expression of h*AGPAT2* resulted in partial regeneration of both white and brown adipose tissue (but only 30%–50% compared with wild-type mice), which had molecular signatures of adipocytes, including leptin secretion. Furthermore, the stromal vascular fraction cells of regenerated adipose depots differentiated *ex vivo* only with doxycycline, suggesting the essential role of *Agpat2* in adipocyte differentiation. Turning off expression of h*AGPAT2 in vivo* resulted in total loss of regenerated adipose tissue, clear evidence that Agpat2 is essential for adipocyte differentiation *in vivo*.

INTRODUCTION

Adipose tissue (AT) is not critical for mammalian development and life; however, it is essential for proper metabolic homeostasis. This is borne out by the fact that humans with autosomal recessive congenital generalized lipodystrophy (CGL) are born with near-total loss of AT.[1–3] Although subjects with CGL are predisposed to metabolic complications of insulin resistance early in life, some of them reportedly live well beyond the 5th or 6th decade of life. Early onset of diabetes mellitus, hepatic steatosis, and hypertriglyceridemia in patients with CGL suggests a clear role of AT in the proper functioning of intermediary metabolism.

Previously, we reported biallelic-disease-causing variants in *AGPAT2* in patients with CGL, type 1 (CGL1).[4] AGPAT2 (1-acylglycerol-3-phosphate O-acyltransferase 2) is an enzyme that converts lysophosphatidic acid (LPA) to phosphatidic acid (PA). PA is a substrate for the biosynthesis of other phospholipids such as phosphatidylcholine (PC), phosphatidylethanolamine (PE), phosphatidylserine (PS), and phosphatidylinositol (PI), as well as for neutral lipids such as diacylglycerol (DAG) and triacylglycerol (TAG).[5,6] To study the underlying mechanisms by which AGPAT2 deficiency results in a near-total loss of AT in humans, we generated a murine model of CGL1 by homozygous deletion of *Agpat2* that recapitulated all the features of human CGL1.[7] The adult *Agpat2*$^{-/-}$ mice have no visually detectable white AT (WAT) or brown AT (BAT),[7] thus precluding us to study the underlying molecular defects resulting in total loss of AT. Previously, we reported that the newborn (P0.5) *Agpat2*$^{-/-}$ mice had some AT in the interscapular region (anatomical region for the location of BAT).[8] Induction of the stromal vascular fraction (SVF) cells from the interscapular region of P0.5 *Agpat2*$^{-/-}$ mice with a cocktail of differentiation factors revealed only reduced differentiation, as well as a lack of caveolae.[9] Most importantly, these differentiated cells did not show the presence of *Ucp1*, a *bona fide* molecular marker for brown adipocytes.[10] The mouse embryonic fibroblasts (MEF) from the *Agpat2*$^{-/-}$ mice (E18.5) also have the ability to differentiate but have reduced adipocyte-like features. It is possible the tissue obtained from the anatomically authentic location for BAT is not true BAT but does have some features of adipocytes—such as accumulating lipids. Previous studies in cultured cells (OP9,[11] 3T3-L1[12]) using a knockdown strategy, and muscle-derived multipotent cells (MDMCs) obtained from vastus lateralis muscle harboring biallelic *AGPAT2* mutations,[12] suggest that *Agpat2* might have a dual role, both in differentiation and likely TAG synthesis.

To determine the role of Agpat2 in the biology of AT and in whole-animal metabolic disease, we re-expressed human AGPAT2 (open reading frame [ORF] corresponding to the expression of full-length protein) regulated by doxycycline specifically in AT (regulated by

[1]Section of Nutrition and Metabolic Diseases, Division of Endocrinology, Department of Internal Medicine, UT Southwestern Medical Center, Dallas, TX 75390, USA
[2]Center for Human Nutrition, UT Southwestern Medical Center, Dallas, TX 75390, USA
[3]Department of Molecular Genetics, UT Southwestern Medical Center, Dallas, TX 75390, USA
[4]Peter O'Donnell Jr. School of Public Health, UT Southwestern Medical Center, Dallas, TX 75390, USA
[5]Touchstone Center for Diabetes Research, UT Southwestern Medical Center, Dallas, TX 75390, USA
[6]Lead contact
*Correspondence: anil.agarwal@utsouthwestern.edu
https://doi.org/10.1016/j.isci.2023.107806

This is an open access article under the CC BY-NC-ND license (http://creativecommons.org/licenses/by-nc-nd/4.0/).

adiponectin promoter) in the *Agpat2*$^{-/-}$ mice. Our current strategy now allows us to evaluate the regenerated AT depots and thus *Agpat2*'s role in the biology of AT. This study describes the generation of transgenic mice re-expressing human AGPAT2 (hAGPAT2) in the *Agpat2*$^{-/-}$ background and shows the regeneration of WAT and BAT depots, but surprisingly only 30%–50% of the AT mass as compared with the age-matched WT mice. The generation-degeneration of AT *in vivo* will also be helpful in studying how the AT is modulated in the current epidemic of obesity. The findings described here are part of a larger study showing amelioration of hepatic steatosis in **Tg-**$^{\text{AT-hA2}}$**;mA2**$^{-/-}$ mice with regenerated adipose tissue. In addition, we find that wild-type (WT) mice overexpressing h*AGPAT2* in adipose tissue have no significant increase in adipose tissue TAG synthesis. These findings will be presented later in the same journal or elsewhere.

RESULTS

Generation of transgenic AGPAT2 mouse model

We generated transgenic mice expressing h*AGPAT2* directed by an AT-specific promoter, adiponectin, which is regulated by a doxycycline inducible system. To accomplish this AT-specific re-expression of h*AGPAT2*, we required generation and multiple crossing of three mouse lines: (1) a mouse strain expressing h*AGPAT2* driven by TRE-tight/P_{min}CMV promoter system; (2) a mouse strain expressing rtTA driven by an adiponectin promoter[13,14]; and (3) an *Agpat2*$^{+/-}$ mouse strain. For detailed generation of mice, see Figures S1A–S1E.

A precise expression profile of fetal adiponectin in mice is unclear. However, a few studies employing immunohistological, *in situ* hybridization, and RT-qPCR techniques show that transcripts for adiponectin are detected on day E16.5 but not on day E12.5 or E14.5.[15,16] A population of proliferating preadipoctyes (*Pdgfr2*$^{+}$) was detected in inguinal white adipose tissue (WAT) depot at E16.5.[17] Another study corroborates these observations where expression of adiponectin was undetectable until E17.5, pinning E16.5 as the earliest day detectable.[18] Adiponectin expression in human fetal tissues is detectable from 14 to 36 weeks of gestation.[19] Given the gestation period of ~21 days (3 weeks) for mice, and 40 weeks for humans, adiponectin expression begins much earlier in human fetuses than in mice. For this study, we chose to turn on hAGPAT2 expression on day E13.5, taking into account the time taken for passage of doxycycline from the placenta to the developing embryos so we do not miss the earliest turn on point for adiponectin expression and remain within the time period of the adiponectin-driven expression of hAGPAT2.

Doxycycline (dox)-fed Tg-$^{\text{AT-hA2}}$;mA2$^{-/-}$ mice regenerate adipose tissue

Initially, regeneration of AT was evaluated in **Tg-**$^{\text{AT-hA2}}$**;m*A2***$^{-/-}$ mice by noninvasive magnetic resonance imaging (MRI) at 12 weeks (Figures S2A–S2C). Only one male mouse per genotype (chow- and dox-fed) at 15 weeks was evaluated by this method, and it was difficult to ascertain the presence of adipose tissue in the **Tg-**$^{\text{AT-hA2}}$**;mA2**$^{-/-}$ mice (Figures S2A–S2C). The percentage of adipose tissue was calculated by magnetic resonance spectroscopy (MRS). The adipose tissue in the WT chow-fed mouse is 16%. Although the adipose tissue peak in the **Tg-**$^{\text{AT-hA2}}$**;mA2**$^{-/-}$ chow-fed mouse is calculated at 5%, the peak is relatively undetectable and could be picking up the hepatic fat. Although a similar AT percentage is calculated for **Tg-**$^{\text{AT-hA2}}$**;mA2**$^{-/-}$ dox-fed mouse, the peak is more prominent; this corroborates our later findings that the regenerated SubQ adipose tissue is not adequate to be measured by MRI and MRS methods (Figures S2A–S2C).

We next sacrificed a few of these mice to inspect AT visually, as shown in Figures 1A–1F and 1J–1O, and weighed SubQ, gonadal, and BAT adipose depots in both sexes at 12 weeks (Figures 1G–1I and 1P–1R). We also obtained representative images of chow-fed **Tg-**$^{\text{AT-hA2}}$**;m*A2***$^{-/-}$, shown in Figure S2D, as an example of mice that completely lack these fat depots. In addition, we show the perirenal and retroperitoneal AT depots in 12 weeks female chow-fed **Tg-**$^{\text{AT-hA2}}$**;mA2**$^{+/+}$ (WT) and **Tg-**$^{\text{AT-hA2}}$**;mA2**$^{-/-}$ mice and dox-fed **Tg-**$^{\text{AT-hA2}}$**;mA2**$^{-/-}$ mice (Figures S3A–S3C). Although the chow-fed **Tg-**$^{\text{AT-hA2}}$**;mA2**$^{-/-}$ mice lack both perirenal and retroperitoneal AT depots, there was some regeneration of both these depots in the dox-fed **Tg-**$^{\text{AT-hA2}}$**;mA2**$^{-/-}$ mice. Other than male gonadal AT, which can be excised distinctly as it sits atop the testes, removing gonadal AT in females, or SubQ/BAT in both males and females, is subjective; therefore, the tissue weight is relative, not absolute. The regeneration of AT at 12 weeks of dox-induced re-expression of *hAGPAT2* was more prominent with the gonadal AT than with SubQ and BAT. The weight of the regenerated AT depots in dox-fed **Tg-**$^{\text{AT-hA2}}$**;mA2**$^{-/-}$ mice was ~30%–50% that of the weight of the corresponding depot in the WT chow-fed mice (Figures 1G–1I and P–R). In addition, when the same AT weight is expressed relative to the animals' body weight at 12 weeks, we note no significant difference between the two methods for expression of the regenerated AT (Figures S3D–S3I). We also have limited data on female dox-fed **Tg-**$^{\text{AT-hA2}}$**;mA2**$^{-/-}$ mice at 24 weeks of age. Here again, even at 24 weeks the regenerated WAT and BAT did not catch-up to the chow-fed **Tg-**$^{\text{AT-hA2}}$**;mA2**$^{+/+}$ mice (Figures S3J–S3O), although confirmatory data will emerge from the male dox **Tg-**$^{\text{AT-hA2}}$**;mA2**$^{-/-}$ mice at 24 weeks of age.

An increase in AT weight is consistent with an increase in plasma leptin levels at 12 weeks (Figures S2E–S2H). In both male and female dox-fed **Tg-**$^{\text{AT-hA2}}$**;m*A2***$^{-/-}$ mice, there is an increase in the plasma leptin levels of 535% and 81%, respectively, compared with chow-fed **Tg-**$^{\text{AT-hA2}}$**;m*A2***$^{-/-}$ mice. However, this did not reach statistical significance most likely due to the wide variation in leptin secretion.

The WAT and BAT from WT and dox-fed **Tg-**$^{\text{AT-hA2}}$**;m*A2***$^{-/-}$ mice of both sexes at 12 weeks were histologically examined for adipocyte number and size (Figures S4A–S4L). We note that in both the white and brown regenerated AT of the dox-fed **Tg-**$^{\text{AT-hA2}}$**;m*A2***$^{-/-}$ mice, the size of the adipocytes are significantly enlarged compared to WT mice. This was also observed in gonadal AT of both sexes at 24 weeks (Figures S4M–S4P). Why there are enlarged adipocytes is unclear. Could it be related to the cellular levels of PA? Although PA and components of the Hippo signaling pathway control cell/organ size, it is only seen in the context of phospholipase D (PLD), which generates plasma-membrane-bound PA.[20,21] How an endoplasmic-reticulum-bound PA (generated by *Agpats*) results in the regulation of cellular/tissue size is unclear. In general, enlarged adipocytes have greater TAG content, although we did not observe increased TAGs in the regenerated adipocytes (described later). The relationship between enlarged adipocytes, TAG content, and physiological function is described in a recent review.[22]

CellPress
OPEN ACCESS

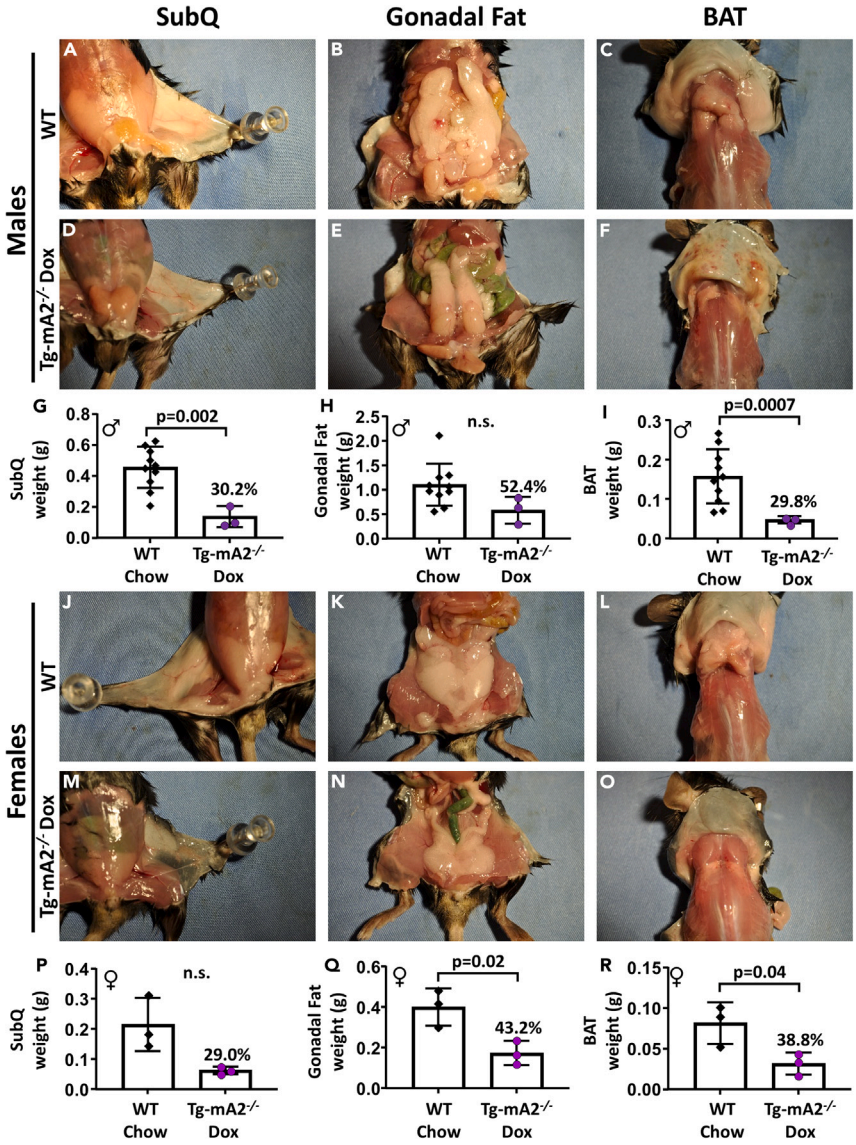

Figure 1. Visual images and weights of adipose tissue depots in Tg-$^{AT\text{-}hA2}$;m*A2*$^{-/-}$ mice

(A and D) Representative visual images for 12-week-old male subcutaneous (SubQ) adipose tissue.

(B and E) Representative visual images for 12-week-old male gonadal adipose tissue.

(C and F) Representative visual images for 12-week-old male brown adipose tissue (BAT).

(J and M) Representative visual images for 12-week-old female SubQ adipose tissue.

(K and N) Representative visual images for 12-week-old female gonadal adipose tissue.

(L and O) Representative visual images for 12-week-old female BAT. All images were acquired using Nikon D5000 with a Nikon DX AFS Nikkor 18-55 mm lens.

(G–I) The male (G) SubQ, (H) gonadal, and (I) BAT adipose tissue depot masses were quantified.

(P–R) The female (P) SubQ, (Q) gonadal, and (R) BAT adipose tissue depots were quantified. Percent adipose tissue regenerated in dox-fed Tg-$^{AT\text{-}hA2}$;m*A2*$^{-/-}$ mice is compared with that in chow-fed WT mice and is shown above the bar. In general, the regenerated adipose tissue depot weight is 30%–50% of the WT levels. The data are represented as mean ± SD. Individual data points are shown within the bars, n = 3–10; p values are shown on the graph, determined using Student's t test. Tg-$^{AT\text{-}hA2}$;m*A2*$^{-/-}$ is abbreviated to Tg-m*A2*$^{-/-}$. The symbols ♂ (male) and ♀ (female) are embedded in the panels. See also Figures S2 and S3.

Differential regeneration of adipose tissue depots could be related to differential expression of mouse and human Agpat2 transcripts

Quantification of the m*Agpat2* transcripts in the chow-fed WT AT depots and h*AGPAT2* transcripts in dox-fed Tg-$^{AT\text{-}hA2}$;m*A2*$^{-/-}$ mice in both sexes are shown in Figures S5A–S5D. Despite SubQ being the lowest expressing and BAT the highest expressing depot for m*Agpat2* in WT mice, we see the most regeneration of AT in the gonadal depot of dox-fed Tg-$^{AT\text{-}hA2}$;m*A2*$^{-/-}$ mice, indicating that there is not a direct

correlation between the expression of m*Agpat2* and AT regeneration. m*Agpat2* is expressed under its own endogenous promoter, whereas the re-expressed h*AGPAT2* is expressed under the adiponectin/Tet-O/CMV promoters and is always on when dox food is provided. It is therefore possible that there are differences in regulating the transcripts between the two promoters in different AT depots.

Measurement of key adipose tissue marker transcripts in Tg-$^{AT\text{-}hA2}$;mA2$^{-/-}$ mice

Re-expression of hAGPAT2 from E13.5 led to regeneration of both white (SubQ and gonadal) and BAT. At 12 weeks, the AT from chow-fed WT and dox-fed Tg-$^{AT\text{-}hA2}$;m*A2*$^{-/-}$ mice of both sexes were excised and analyzed for the transcripts specific to the ATs. Chow-fed Tg-$^{AT\text{-}hA2}$;m*A2*$^{-/-}$ mice do not have AT, so we compared the expression of transcripts from only dox-fed Tg-$^{AT\text{-}hA2}$;m*A2*$^{-/-}$ mice with that from WT (chow-fed) mice. The detection of transcripts specific for adipocyte lineage in dox-fed Tg-$^{AT\text{-}hA2}$;m*A2*$^{-/-}$ mice suggests the presence of *bona fide* adipocytes, but the expression of these transcripts is less than the WT (chow-fed) mice (Table 1). Pref-1, a marker for preadipocytes, was more prominently reduced in BAT and SubQ tissue in dox-fed Tg-$^{AT\text{-}hA2}$;m*A2*$^{-/-}$ mice than in gonadal AT in females but not in males. Despite the molecular signatures of adipocytes in the regenerated tissue, the key enzymes involved in *de novo* lipogenesis in all 3 adipose depots of both sexes were still suppressed more than 2-fold compared with chow-fed WT levels.

As expected, m*Agpat2* is undetectable, as we used *Agpat2*$^{-/-}$ mice as the background for the expression of h*AGPAT2*. In all the AT, the h*AGPAT2* was detected 100-fold more, except in SubQ females where it was noted at ~50-fold. *Dgats* are the ultimate step in the synthesis of TAG, converting DAG to TAG. The expression of *Dgat1* and *Dgat2* remains suppressed in dox-fed Tg-$^{AT\text{-}hA2}$;m*A2*$^{-/-}$ mice compared with chow-fed WT mice, as observed for the *de novo* lipogenesis pathway. These expression changes in regenerated AT in dox-fed Tg-$^{AT\text{-}hA2}$;m*A2*$^{-/-}$ mice suggest that although AT has been regenerated, it is still not mature in terms of *de novo* lipogenesis and TAG synthesis.

Among the several functions of adipose tissue, the main one is to store fatty acids as triacylglycerol (TAG) and to release the fatty acids via the process of lipolysis. The process of lipolysis involves three lipases, ATGL, HSL, and MAGL, which sequentially release the fatty acids from TAG.[23] We measured the mRNA expression of these lipases in all three AT depots. As shown in Table 1, the expression of these transcripts remains suppressed in dox-fed Tg-$^{AT\text{-}hA2}$;m*A2*$^{-/-}$mice compared with the chow-fed Tg-$^{AT\text{-}hA2}$;m*A2*$^{+/+}$ mice for both sexes. The expression level remained suppressed compared with those of Tg-$^{AT\text{-}hA2}$;m*A2*$^{+/+}$ mice at both 12 and 24 weeks (Tables 1 and 2), indicating that generated adipocytes are still not fully matured from the perspective of lipolysis. This observation will also suggest that the decrease in AT weight is not due to increased lipolysis of TAG in the newly generated adipocytes/AT, although it is to be noted that the expression of key TAG biosynthesis enzymes is also not highly expressed. This observation suggests that the newly generated adipocytes/AT have not matured enough to synthesize large quantities of TAG or to degrade TAG.

Very low density lipoproteins (VLDL) are secreted by the liver and is taken-up by the tissues such as adipose, heart, kidneys, and skeletal muscle to be degraded to generate fatty acids. VLDL binds to the VLDL receptor (VLDLR),[24] present in the above tissues. We also measured the expression of VLDLR in the adipose depots to determine whether the generated AT is competent in absorbing the circulating VLDL.[25] We found no difference in the gonadal AT and BAT at both 12 and 24 weeks (Tables 1 and 2). In the SubQ AT, the expression was ~2.5-fold decreased in female dox-fed Tg-$^{AT\text{-}hA2}$;m*A2*$^{-/-}$ mice compared with chow-fed Tg-$^{AT\text{-}hA2}$;m*A2*$^{+/+}$ mice, indicating that the generated AT is functional but at a sub-par level (Tables 1 and 2).

UCPs are the uncoupling proteins that have specific roles in thermogenesis, and *Ucp1* is considered a *bona fide* marker for BAT.[26,27] We measured the transcripts for the three *Ucps* (−1, −2, −3).[28,29] In our assay, we detected *Ucp1* in both male and female BAT of dox-fed Tg-$^{AT\text{-}hA2}$;m*A2*$^{-/-}$ mice (0.41- [male] and 0.19 [female]-fold) but it did not reach the level of expression seen in chow-fed WT mice. *Ucp1* is normally not observed in WAT; however, when WAT obtain a beige-like feature, they do show the presence of *Ucp1*. In the re-expressed WAT in dox-fed Tg-$^{AT\text{-}hA2}$;m*A2*$^{-/-}$ mice, *Ucp1* expression is again not expressed to the same level as in chow-fed WT mice, except a slight increase in male gonadal AT. Interestingly, we also noted the expression of *Ucp2* in BAT, which was higher in dox-fed Tg-$^{AT\text{-}hA2}$;m*A2*$^{-/-}$ mice than chow-fed WT mice. However, the expression of *Ucp2* was not as high as *Ucp1* (avg C_t values 23.5 and 17.3, respectively). In gonadal and SubQ AT, the *Ucp2* expression was equal between dox-fed Tg-$^{AT\text{-}hA2}$;m*A2*$^{-/-}$ mice and chow-fed WT mice. There was no variation in expression of *Ucp3* between the 3 AT depots, but the expression in dox-fed Tg-$^{AT\text{-}hA2}$;m*A2*$^{-/-}$ mice is again suppressed compared with chow-fed WT mice.

We also profiled the transcripts studied at 24 weeks in the AT depots obtained from 24-week-old WT and dox-fed Tg-$^{AT\text{-}hA2}$;m*A2*$^{-/-}$ mice from both sexes. The transcripts for the pathways studied at 24 weeks were qualitatively similar to that of 12-week expression (Table 2).

Increased presence of markers for inflammation in the generated adipose tissue

Normally, the expansion of AT (either by hyperplasia or hypertrophy), as in obesity, attracts macrophage infiltration[30]; this is more common in obese AT than in lean AT. Here though, the regenerated AT of dox-fed Tg-$^{AT\text{-}hA2}$;m*A2*$^{-/-}$ mice from both sexes showed an increase in cell size but not an increase in tissue mass as observed in obesity, which prompted us to measure a few of the inflammatory markers in the generated AT in all three depots of both sexes and both at 12 and 24 weeks. These inflammation markers, interleukin-6 (*Il-6*), tumor necrosis factor alpha (*Tnfα*), *Ccl2*, and *Ccl4*, were selected based on previous reports in obese AT.[31]

At 12 and 24 weeks, *Il-6* is not expressed in either chow-fed Tg-$^{AT\text{-}hA2}$;m*A2*$^{+/+}$ or dox-fed Tg-$^{AT\text{-}hA2}$;m*A2*$^{-/-}$ mice of both sexes. *Ccl4* is not expressed in chow-fed Tg-$^{AT\text{-}hA2}$;m*A2*$^{+/+}$ mice of either sex (C_t>30) but has depot-specific upregulation in the generated adipose tissue of dox-fed Tg-$^{AT\text{-}hA2}$;m*A2*$^{-/-}$ mice (Table 3). A caution is that the fold increase in the dox-fed Tg-$^{AT\text{-}hA2}$;m*A2*$^{-/-}$ mice might not reflect the real increase due to low expression of these markers in chow-fed Tg-$^{AT\text{-}hA2}$;m*A2*$^{+/+}$ mice of either sex. *Ccl2*, another chemokine, is detected in all AT except BAT of chow-fed Tg-$^{AT\text{-}hA2}$;m*A2*$^{+/+}$ mice, increasing by ~1.5-–to 2-fold in SubQ, ~3- to 7-fold in gonadal tissue, and markedly in

Table 1. RT-qPCR measurements of key genes for pathways of adipocyte lineage, *de novo* lipogenesis, triacylglycerol synthesis, fatty acid oxidation, lipolysis, and *Ucps* in adipose tissue of 12 weeks chow-fed WT and doxycycline (dox)-fed Tg-$^{AT\text{-}hA2}$;m$A2^{-/-}$ mice

Tissue	SubQ				Gonadal				BAT			
Sex	Male		Female		Male		Female		Male		Female	
Genotype	WT	Tg-m$A2^{-/-}$	WT	Tg-m$A2^{-/-}$	WT	Tg-m$A2^{-/-}$	WT	Tg-m$A2^{-/-}$	WT	Tg-m$A2^{-/-}$	WT	Tg-m$A2^{-/-}$
Diet	Chow	Dox	Chow	Dox	Chow	Dox	Chow	Dox	Chow	Dox	Chow	Dox
# of samples pooled	4	4	4	4	3	4	4	4	4	4	4	4
Gene/Fold Change												
Adipocyte Lineage												
Ap2	1.00	0.58	1.00	0.11	1.00	0.50	1.00	0.23	1.00	0.54	1.00	0.29
Cebpα	1.00	0.29	1.00	0.11	1.00	0.33	1.00	0.10	1.00	0.27	1.00	0.33
Pparγ	1.00	0.53	1.00	0.10	1.00	0.35	1.00	0.25	1.00	0.27	1.00	0.20
Perilipin 1	1.00	0.34	1.00	0.07	1.00	0.32	1.00	0.17	1.00	0.30	1.00	0.25
Pref. 1	1.00	**0.53**	**1.00**	**0.46**	1.00	0.21	1.00	1.14	1.00	**0.80**	1.00	**0.50**
De Novo Lipogenesis												
Acc1	1.00	0.09	1.00	0.03	1.00	0.33	1.00	0.05	1.00	0.22	1.00	0.24
Acc2	1.00	0.18	1.00	**0.02**	1.00	0.37	1.00	0.04	1.00	0.31	1.00	0.29
Acly	1.00	0.10	1.00	0.04	1.00	0.58	1.00	0.05	1.00	0.24	1.00	0.27
Elovl6	1.00	0.07	1.00	0.03	1.00	0.50	1.00	0.04	1.00	0.25	1.00	0.27
Fas	1.00	0.09	1.00	0.03	1.00	0.44	1.00	0.05	1.00	0.25	1.00	0.21
Scd 1	1.00	0.13	1.00	0.05	1.00	0.25	1.00	0.12	1.00	0.21	1.00	0.36
Scd 2	1.00	0.46	1.00	0.27	1.00	1.05	1.00	0.37	1.00	0.54	1.00	0.69
Triacylglycerol Synthesis												
hAgpat2	1.00	338.88	1.00	51.05	1.00	306.81	1.00	104.54	1.00	744.42	1.00	393.72
mAgpat2	1.00	0.00	1.00	**0.00**	1.00	0.00	1.00	0.00	1.00	0.00	1.00	0.04
mAgpat10	1.00	1.37	1.00	0.11	1.00	0.21	1.00	0.18	1.00	0.45	1.00	0.35
Mogat1	1.00	0.31	1.00	**0.04**	1.00	0.15	1.00	**0.05**	1.00	0.52	1.00	0.26
Mogat2	1.00	1.62	1.00	**0.33**	1.00	1.90	1.00	0.59	**1.00**	5.37	1.00	1.34
Dgat1	1.00	0.39	1.00	0.27	1.00	0.43	1.00	0.29	1.00	0.44	1.00	0.35
Dgat2	1.00	0.60	1.00	0.14	1.00	0.90	1.00	0.27	1.00	0.30	1.00	0.17

(*Continued on next page*)

CellPress
OPEN ACCESS

Table 1. *Continued*

Tissue	SubQ				Gonadal				BAT			
Sex	Male		Female		Male		Female		Male		Female	
Fatty Acid Oxidation												
Pparα	1.00	0.07	1.00	**0.02**	1.00	**0.25**	1.00	0.16	1.00	0.32	1.00	0.24
Cpt1a	1.00	1.02	1.00	0.93	1.00	1.12	1.00	1.68	1.00	1.43	1.00	2.22
Cpt1b	1.00	0.16	1.00	0.08	1.00	1.62	1.00	0.23	1.00	0.63	1.00	0.54
Cpt2	1.00	0.33	1.00	0.19	1.00	0.53	1.00	0.27	1.00	0.55	1.00	0.47
Acox1	1.00	0.53	1.00	0.23	1.00	0.72	1.00	0.39	1.00	0.53	1.00	0.53
Mcad	1.00	0.42	1.00	0.16	1.00	0.62	1.00	0.28	1.00	0.50	1.00	0.32
Vlcad	1.00	0.51	1.00	**0.18**	1.00	0.97	1.00	0.21	1.00	0.83	1.00	0.28
Ucp1	1.00	0.05	1.00	**0.001**	**1.00**	**2.49**	1.00	0.05	1.00	0.41	1.00	0.19
Ucp2	1.00	1.37	1.00	0.87	1.00	1.81	1.00	1.20	1.00	1.79	1.00	2.05
Ucp3	1.00	0.30	1.00	**0.06**	1.00	0.86	1.00	0.17	1.00	0.55	1.00	0.31
Lipolysis												
Atgl	1.00	0.40	1.00	0.08	1.00	0.40	1.00	0.20	1.00	0.23	1.00	0.30
Hsl	1.00	0.38	1.00	0.09	1.00	0.34	1.00	0.24	1.00	0.29	1.00	0.32
Mgll	1.00	0.72	1.00	0.12	1.00	0.54	1.00	0.31	1.00	0.43	1.00	0.46
Lipid Particle Uptake												
Vldlr	1.00	0.68	1.00	0.37	1.00	0.80	1.00	0.88	1.00	0.76	1.00	0.85

An equal quantity of total RNA was pooled from each mouse (n = 3–4) and quantified once in duplicate. Data are shown compared with chow-fed WT mice = 1. Bold text indicates a raw C_t value >30. Wherever the raw C_t value >30, we consider the fold change as approximate. For the human transgene *hAGPAT2*, the raw C_t values are as follows: in male subcutaneous tissue, chow-fed C_t = 26.03, dox-fed C_t = 18.32; in gonadal tissue, chow-fed C_t = 25.28, dox-fed C_t = 16.15; in brown adipose tissue, chow-fed C_t = 26.44, dox-fed C_t = 17.23. C_t values were similar for the females. SubQ, subcutaneous adipose tissue; gonadal, gonadal adipose tissue; BAT, brown adipose tissue. WT Tg-$^{AT\text{-}hA2}$;m$A^{+/+}$ is abbreviated to Tg-m$A2^{+/+}$. Tg-$^{AT\text{-}hA2}$;m$A2^{-/-}$ is abbreviated to Tg-m$A2^{-/-}$. See also Table S1.

Table 2. RT-qPCR measurements of key genes for pathways of adipocyte lineage, *de novo* lipogenesis, triacylglycerol synthesis, fatty acid oxidation, lipolysis, and *Ucps* in adipose tissue of 24 weeks chow-fed WT and doxycycline (dox)-fed Tg-$^{AT\text{-}hA2}$;m$A2^{-/-}$ mice

Tissue	SubQ				Gonadal				BAT			
Sex	Male		Female		Male		Female		Male		Female	
Genotype	WT	Tg-m$A2^{-/-}$	WT	Tg-m$A2^{-/-}$	WT	Tg-m$A2^{-/-}$	WT	Tg-m$A2^{-/-}$	WT	Tg-m$A2^{-/-}$	WT	Tg-m$A2^{-/-}$
Diet	Chow	Dox	Chow	Dox	Chow	Dox	Chow	Dox	Chow	Dox	Chow	Dox
# of samples pooled	3	4	5	2	3	4	5	5	3	3	5	5
Gene/Fold Change												
Adipocyte Lineage												
Ap2	1.00	2.19	1.00	0.15	1.00	0.30	1.00	0.47	1.00	0.53	1.00	1.83
Cebpα	1.00	0.78	1.00	0.10	1.00	0.17	1.00	0.11	1.00	0.30	1.00	0.37
Pparγ	1.00	1.78	1.00	0.09	1.00	0.23	1.00	0.18	1.00	0.28	1.00	0.61
Perilipin 1	1.00	1.27	1.00	0.07	1.00	0.14	1.00	0.12	1.00	0.88	**1.00**	**0.50**
Pref. 1	**1.00**	**4.72**	**1.00**	**0.76**	**1.00**	**0.35**	**1.00**	**2.77**	**1.00**	**1.34**	**1.00**	**1.78**
De Novo Lipogenesis												
Acc1	1.00	0.72	1.00	0.07	1.00	0.29	1.00	0.07	1.00	0.45	1.00	0.64
Acc2	1.00	0.43	1.00	**0.04**	1.00	0.20	1.00	**0.05**	1.00	0.35	1.00	0.53
Acly	1.00	1.06	1.00	0.13	1.00	0.74	1.00	0.22	1.00	0.96	1.00	1.51
Elovl6	1.00	0.40	1.00	0.08	1.00	1.66	1.00	0.10	1.00	0.57	1.00	0.79
Fas	1.00	1.27	1.00	0.05	1.00	1.12	1.00	0.10	1.00	0.70	1.00	0.80
Scd 1	1.00	0.69	1.00	0.13	1.00	0.18	1.00	0.20	1.00	0.39	1.00	1.95
Scd 2	1.00	4.25	1.00	1.10	1.00	2.58	1.00	0.90	1.00	1.92	1.00	2.13
Triglyceride Synthesis												
hAgpat2	**1.00**	1479.22	1.00	153.57	1.00	191.31	1.00	95.63	**1.00**	697.73	1.00	353.71
mAgpat2	1.00	**0.00**	1.00	0.01	1.00	**0.00**	1.00	**0.00**	1.00	**0.00**	1.00	**0.00**
mAgpat10	1.00	1.44	1.00	0.07	1.00	0.16	1.00	**0.07**	1.00	0.40	1.00	0.25
Mogat1	**1.00**	1.04	1.00	**0.04**	1.00	0.09	1.00	**0.03**	1.00	**0.27**	1.00	**0.35**
Mogat2	**1.00**	17.11	**1.00**	**1.22**	**1.00**	1.06	1.00	**0.61**	**1.00**	**0.36**	1.00	**0.88**
Dgat1	1.00	0.49	1.00	**0.35**	1.00	0.21	1.00	**0.24**	1.00	0.41	1.00	1.03
Dgat2	1.00	3.41	1.00	0.37	1.00	0.51	1.00	0.16	1.00	0.33	1.00	0.45

(*Continued on next page*)

CellPress
OPEN ACCESS

Table 2. *Continued*

Tissue	SubQ				Gonadal				BAT			
Sex	Male		Female		Male		Female		Male		Female	
Fatty Acid Oxidation												
Pparα	1.00	**0.18**	1.00	**0.05**	1.00	**0.14**	1.00	**0.19**	1.00	0.20	1.00	0.55
Cpt1a	1.00	2.05	1.00	0.69	1.00	0.60	1.00	1.09	1.00	1.49	1.00	**1.05**
Cpt1b	1.00	0.31	1.00	0.28	1.00	0.81	1.00	**0.25**	1.00	0.43	1.00	0.67
Cpt2	1.00	1.33	1.00	0.18	1.00	0.20	1.00	0.24	1.00	0.72	1.00	0.96
Acox1	1.00	1.55	1.00	0.23	1.00	0.23	1.00	0.27	1.00	0.44	1.00	0.73
Mcad	1.00	1.14	1.00	0.17	1.00	0.23	1.00	0.25	1.00	0.47	1.00	0.61
Vlcad	1.00	1.97	1.00	0.25	1.00	0.60	1.00	0.19	1.00	0.81	1.00	0.60
Ucp1	1.00	**0.02**	1.00	**0.03**	1.00	0.06	1.00	0.04	1.00	0.33	1.00	0.61
Ucp2	1.00	0.85	1.00	1.21	1.00	1.68	1.00	1.01	1.00	2.30	1.00	1.66
Ucp3	1.00	0.73	1.00	**0.15**	1.00	0.19	1.00	0.20	1.00	0.50	1.00	0.34
Lipolysis												
Atgl	1.00	1.12	1.00	0.06	1.00	0.18	1.00	0.12	1.00	0.38	1.00	0.60
Hsl	1.00	1.07	1.00	0.09	1.00	0.17	1.00	0.13	1.00	0.42	1.00	0.63
Mgll	1.00	2.01	1.00	0.14	1.00	0.41	1.00	0.27	1.00	0.46	1.00	0.77
Lipid Particle Uptake												
Vldlr	1.00	2.22	1.00	0.38	1.00	0.75	1.00	0.94	1.00	1.93	1.00	0.86

An equal quantity of total RNA was pooled from each mouse (n = 3–6) and quantified once in duplicate. Data are shown compared with chow-fed WT mice = 1. Bold text indicates a raw C_t value >30. Wherever the raw C_t value >30, we consider the fold change as approximate. For the human transgene hAGPAT2, the raw C_t values are as follows: in male SubQ, chow-fed C_t = 31.12, dox-fed C_t = 19.58; in gonadal tissue, chow-fed C_t = 28.16, dox-fed Ct = 19.49; in brown adipose tissue, chow-fed C_t = 30.80, dox-fed C_t = 21.13. C_t values were similar for the females. SubQ, subcutaneous adipose tissue; gonadal, gonadal adipose tissue; BAT, brown adipose tissue. **WT Tg-$^{AT\text{-}hA2}$;mA$^{+/+}$** is abbreviated to **Tg-mA2$^{+/+}$**. Tg-$^{AT\text{-}hA2}$;mA2$^{-/-}$ is abbreviated to Tg-mA2$^{-/-}$. See also Table S1.

CellPress
OPEN ACCESS

Table 3. RT-qPCR measurements of select genes for inflammation in adipose tissue depots of 12 and 24 weeks chow-fed WT and doxycycline (dox)-fed Tg-$^{AT\text{-}hA2}$;mA2$^{-/-}$ mice

	12 weeks				24 weeks			
Sex	Male		Female		Male		Female	
Genotype	WT	Tg-mA2$^{-/-}$	WT	Tg-mA2$^{-/-}$	WT	Tg-mA2$^{-/-}$	WT	Tg-mA2$^{-/-}$
Diet	Chow	Dox	Chow	Dox	Chow	Dox	Chow	Dox
Tissue	SubQ							
# of samples pooled	4	4	4	4	3	4	5	2
Gene/Fold Change								
Il-6	**1.00**	**1.24**	**1.00**	**2.39**	**1.00**	**1.92**	**1.00**	**0.52**
Ccl2	1.00	1.88	1.00	1.60	1.00	2.12	1.00	2.40
Tnfα	1.00	2.71	1.00	1.04	**1.00**	1.32	1.00	2.89
Ccl4	**1.00**	2.41	**1.00**	**1.60**	**1.00**	**1.14**	**1.00**	**2.16**
Tissue	Gonadal							
# of samples pooled	3	4	4	4	3	4	5	5
Il-6	**1.00**	**2.69**	**1.00**	**4.08**	**1.00**	**2.98**	**1.00**	**4.49**
Ccl2	1.00	3.16	1.00	**6.50**	1.00	6.88	1.00	2.76
Tnfα	**1.00**	10.24	**1.00**	**1.36**	**1.00**	8.37	**1.00**	**1.05**
Ccl4	**1.00**	4.58	**1.00**	7.82	**1.00**	5.74	**1.00**	**5.71**
Tissue	BAT							
# of samples pooled	4	4	4	4	3	3	5	5
Il-6	**1.00**	**16.10**	**1.00**	**4.78**	**1.00**	**1.38**	**1.00**	**4.81**
Ccl2	**1.00**	7.71	**1.00**	10.35	**1.00**	5.62	**1.00**	10.35
Tnfα	**1.00**	**13.19**	**1.00**	**5.61**	**1.00**	**14.22**	**1.00**	**8.27**
Ccl4	**1.00**	**6.43**	**1.00**	**15.27**	**1.00**	**6.66**	**1.00**	**5.36**

An equal quantity of total RNA was pooled from each mouse (n = 3–4) and quantified once in duplicate. Data are shown compared with chow-fed WT mice = 1. Bold text indicates a raw C_t value >30. Wherever the raw C_t value >30, we consider the fold change as approximate. SubQ, subcutaneous adipose tissue; gonadal, gonadal adipose tissue; BAT, brown adipose tissue. Tg-$^{AT\text{-}hA2}$;mA$^{+/+}$ is abbreviated to WT. Tg-$^{AT\text{-}hA2}$;mA2$^{-/-}$ is abbreviated to Tg-mA2$^{-/-}$. See also Table S1.

BAT (7- to 10-fold) of dox-fed Tg-$^{AT\text{-}hA2}$;mA2$^{-/-}$ mice. This pattern is also observed with the expression of *Tnfα*. The presence of these inflammatory markers in regenerated AT depots of dox-fed Tg-$^{AT\text{-}hA2}$;mA2$^{-/-}$ mice would indicate potentially dysfunctional adipose tissue. Inflammation from dying cells can attract adipose tissue macrophages (ATMs) in order to remove the dead adipocytes. However, we did not observe increased dead cells when measured by TUNEL labeling at 12 weeks old (discussed below).

Because the generated AT in dox-fed Tg-$^{AT\text{-}hA2}$;mA2$^{-/-}$ mice is only ~50% of the chow-fed Tg-$^{AT\text{-}hA2}$;mA2$^{+/+}$ mice (certainly not demonstrating a high level of hyperplasia/hypertrophy), it was surprising to note the increase in the markers of inflammation. A prior investigation has reported that the presence/recruitment of monocytes/macrophages is critical in the development/maintenance of AT.[32] In another study where human adipose-derived stem cells and human umbilical vein endothelial cells were co-cultured, *Ccl2* was essential for adipogenesis and angiogenesis.[33] Additional studies are required to show that inadequate regeneration of AT in dox-fed Tg-$^{AT\text{-}hA2}$;mA2$^{-/-}$ mice is due to inadequate angiogenesis. This observation would suggest a possibility of inadequate development of vascularization for the generating AT. Not studied and measured here is whether AT vasculature is dependent on the expression of AGPAT2.

Tandem mass Tag-mass spectrometry (TMT-MS) measurements

To complement the mRNA expression, we measured the proteins in 12-week-old male adipose tissue lysates from dox-fed *Tg-$^{AT\text{-}hA2}$;mA2$^{-/-}$* and compared with those from 12-week chow-fed *Tg-$^{AT\text{-}hA2}$;mA2$^{+/+}$* mice employing TMT-MS.[34,35] We employed this method (1) to measure several proteins from limited tissue samples and (2) to identify protein-specific peptides, eliminating the need to use highly characterized antibodies, which are not available for all proteins. As shown in Table 4, human AGPAT2 transgene expression was increased several fold (10- to 18-fold) in dox-fed *Tg-$^{AT\text{-}hA2}$;mA2$^{-/-}$* compared with chow-fed *Tg-$^{AT\text{-}hA2}$;mA2$^{+/+}$* mice in all three AT depots, which is consistent with the increased expression of mRNA (Table 1). We also noted differential protein expression among the three adipose depots. Elovl6 was not detected in WAT but was detected in BAT. Mogat1 was not detected in gonadal AT or BAT but was detected in SubQ AT. Cpt1b, Ucp1, and Ucp3 were undetectable only in gonadal AT but detected in SubQ AT and BAT. A few proteins could not be detected by this method, although they were present by mRNA.

Table 4. Protein measurements of select proteins in adipose tissue depots of 12 weeks chow-fed WT and doxycycline (dox)-fed Tg-$^{AT\text{-}hA2}$;m*A2*$^{-/-}$ male mice by tandem mass tag (TMT) mass spectrometry (TMT-MS)

Tissue			SubQ				Gonadal				BAT			
Genotype					WT	Tg-m*A2*$^{-/-}$			WT	Tg-m*A2*$^{-/-}$			WT	Tg-m*A2*$^{-/-}$
Protein name	Protein Accession	Peptide sequence [AA-AA]	PSM	Unique peptide #	Chow (n=3)	Dox (n=3)	PSM	Unique peptide #	Chow (n=3)	Dox (n=3)	PSM	Unique peptide #	Chow (n=3)	Dox (n=3)
					Fold Change				Fold Change				Fold Change	
Adipocyte Lineage														
Ap2	*P04117*	*SIITLDGGALVQVQK [83–97]*	*2071*	*14*	1.00	0.16*	2790	18	1.00	0.59	2216	17	1.00	0.34$
Cebpα	*P53566*	*TGGGGGGSGAGAGK [261–274]; VLELTSDNDR [315–324]*	*1*	*1*	1.00	0.23	4	2	1.00	0.56	1	1	1.00	0.34*
Perilipin 1	*Q8CGN5*	*ETAEYAANTR [159–168]*	*172*	*31*	1.00	0.38	171	29	1.00	1.24	329	33	1.00	0.47
De Novo Lipogenesis														
Acc1	*Q5SWU9*	*IIQQAGQVWFPDSAFK [2009–2024]*	*251*	*69*	1.00	0.41	236	66	1.00	3.24	1398	120	1.00	0.22‡
Acc2	*E9Q4Z2*	*LLYGESPWGVTPIPFETPLSPPIAR [611–635]*	*68*	*8*	1.00	0.42	63	11	1.00	2.59	593	85	1.00	0.26‡
Acly	*Q91V92*	*GQELIYAGMPITEVFK [839–854]*	*514*	*67*	1.00	0.18	573	67	1.00	0.77	3103	81	1.00	0.18‡
Elovl6	Q920L5	QFNENEAIQWMQENWK [16–31]	ND	ND	ND	ND	ND	ND	ND	ND	21.00	3.00	1.00	0.31
Fas	*P19096*	*LLLEVSYEAIVDGGINPASLR [81–101]*	*2174*	*142*	1.00	0.15	2137	139	1.00	1.04	7817	160	1.00	0.15$
Scd 1	*P13516*	*EDIHDPTYQDEEGPPPK [48–64]*	*19*	*3*	1.00	0.22*	15	3	1.00	0.72	67	6	1.00	0.28
Scd 2	*P13011*	*TGDGSCK [350–356]*	*4*	*1*	1.00	0.44	3	1	1.00	0.87	26	2	1.00	0.40
Triacylglycerol Synthesis														
hAgpat2	*O15120*	*SSTAMTVMADLGER [146–159]*	*52*	*5*	1.00	10.34*	64	7	1.00	18.73‡	79	8	1.00	17.17*
mAgpat2	*Q8K3K7*	*VQVLDAVPTNGLTDADVTK [225–243]*	*41*	*8*	1.00	0.05	27	5	1.00	0.07*	86	11	1.00	0.06
mAgpat10	*Q8C0N2*	*YNPQFGDAFWNSSK [333–346]*	*22*	*9*	1.00	0.72	20	8	1.00	1.72	11	5	1.00	1.45
Mogat1	*Q91ZV4*	*TPEQGGR [64–70]*	*1*	*1*	1.00	0.36*	ND	ND	ND	ND	ND	ND	ND	ND
Dgat1	*Q9Z2A7*	*VSGAAAQQAVSYPDNLTYR [243–261]*	*30*	*10*	1.00	0.28*	19	10	1.00	0.92	40	13	1.00	0.33‡
Dgat2	*Q9DCV3*	*QVIFEEGSWGR [287–297]*	*6*	*2*	1.00	0.75	6	4	1.00	1.52	14	6	1.00	1.06
Fatty Acid Oxidation														
Cpt1a	*P97742*	IPGEETDTIQHVK [317–329]	*29*	*13*	1.00	1.95	29	13	1.00	4.24‡	21	7	1.00	1.56
Cpt1b	*Q924X2*	*TSPDAFVQIALQLAHFR [564–580]*	*12*	*8*	1.00	0.28	ND	ND	ND	ND	184	29	1.00	0.56
Cpt2	*P52825*	*GVTLPELYQDPAYQR [567–581]*	*109*	*30*	1.00	0.29*	88	27	1.00	1.11	239	35	1.00	0.41*
Acox1	*Q9R0H0*	*EIENLILNDPDFQHEDYNFLTR [35–56]*	*189*	*37*	1.00	0.43$	274	40	1.00	1.99	174	31	1.00	0.95
Mcad	*P45952*	*QEPGLGFSFELTEQQK [31–46]*	*158*	*26*	1.00	0.20‡	212	29	1.00	0.84	661	35	1.00	0.28$
Vlcad	*P50544*	*EATQAVLDKPETLSSDASTR [44–63]*	*155*	*38*	1.00	0.30*	116	36	1.00	1.00	927	48	1.00	0.41*

(Continued on next page)

Table 4. *Continued*

Tissue			SubQ				Gonadal				BAT			
Genotype					WT	Tg-m*A2*$^{-/-}$			WT	Tg-m*A2*$^{-/-}$			WT	Tg-m*A2*$^{-/-}$
Ucp1	*P12242*	*GVLGTITTLAK [57–67]*	*6*	*3*	1.00	0.30	ND	ND	ND	ND	626	21	1.00	0.81
Ucp3	*P56501*	*FLGAGTAACFADLLTFPLDTAK [17–38]; GTMDAYR [157–163]*	*2*	*1*	1.00	0.28‡	ND	ND	ND	ND	21	9	1.00	0.66
Lipolysis														
Atgl	*Q8BJ56*	*YVDGGISDNLPLYELK [164–179]*	*24*	*9*	1.00	0.23*	25	11	1.00	1.06	77	18	1.00	0.25‡
Hsl	*P54310*	*VPDGIMAAYPVTTLQSSASPSR [443–464]*	*148*	*31*	1.00	0.40	162	33	1.00	1.56	224	40	1.00	0.04$
Mgll	*O35678*	*DVLQHVDTIQK [115–125]*	*85*	*17*	1.00	0.36‡	86	17	1.00	1.21	81	18	1.00	0.80
Lipid particle uptake														
Vldlr	*P98156*	*EPASIAVDPLSGFVYWSDWGEPAK [557–580]*	*7*	*4*	1.00	0.36‡	6	4	1.00	1.19	14	8	1.00	0.50‡

Shown are the fold changes in the proteins between the chow-fed WT and dox-fed Tg-$^{AT\text{-}hA2}$;m*A2*$^{-/-}$ mice. The TMT-MS data were first normalized by total ion species for each sample, followed by a ratio of protein to cyclophilin. Shown is a representative unique peptide that was detected for each protein consistent for all three adipose depots, except for Cebpα and Ucp3, where 2 peptides are listed. The fold change shown for hAGPAT2 in dox-fed Tg-$^{AT\text{-}hA2}$;m*A2*$^{-/-}$ mice is an approximate fold change, as the human Agpat2 transgene is not expressed in chow-fed WT mice; p values are indicated with symbols where significant, determined using one-way ANOVA. *: $p < 0.05$, ‡: $p < 0.01$, $: $p < 0.001$. PSM, peptide-spectrum match; AA, amino acid; ND, not detected; SubQ, subcutaneous adipose tissue; gonadal, gonadal adipose tissue; BAT, brown adipose tissue. **WT Tg-m*A2*$^{+/+}$**. **Tg-$^{AT\text{-}hA2}$;m*A2*$^{-/-}$** is abbreviated to **Tg-m*A2*$^{-/-}$**.

CellPress
OPEN ACCESS

The stromal vascular fraction cells from regenerated adipose tissue in dox-fed Tg-$^{AT\text{-}hA2}$;m*A2*$^{-/-}$ mice differentiate to mature adipocytes and accumulate lipids upon induction

The stromal vascular fraction (SVF) cells have the potential to differentiate to mature adipocytes. To determine the SVF cell differentiation potential from dox-fed Tg-$^{AT\text{-}hA2}$;m*A2*$^{-/-}$ mice, we set up induction of SVF cells to mature adipocytes in the three AT depots studied from both sexes. We maintained the cells from dox-fed Tg-$^{AT\text{-}hA2}$;m*A2*$^{-/-}$ mice in either the presence or the absence of doxycycline in the culture media, to examine the effects of the expression of hAGPAT2 on differentiation. We encountered difficulties in differentiating the gonadal SVF cells of both sexes. In our efforts to optimize the differentiation, we used various changes in the differentiation protocols, including (1) changes in the serum (different FBS serum lots, animal sources: bovine and mouse), (2) cocktail recipes (including adding LPA [18:1] and PA [18:1_18:1 (DOPA)] to the induction cocktail), (3) ages of mice sacrificed, and (4) fluorescence-activated cell sorting (FACS) for CD31^{+}, CD34^{+}, and CD45^{+} cells. In some experiments, we added doxycycline to the media either immediately before induction or from the day of isolation from the mice to ensure the expression of the h*Agpat2* transgene. When we used mouse plasma (isolated in house), the gonadal cells seemed to differentiate better. However, we cannot reproduce this because mouse plasma is not conveniently available. We tried mouse serum instead but did not see any induction.

These changes were done under consistent cell plating on 12-well collagen-coated plates with a duration of cellular differentiation of 8 days. The Oil Red O (ORO) staining method remained the same throughout. We noted in our differentiation protocol that despite the cells being plated on collagen-coated plates, the gonadal SVF cells had a tendency to *peel off the plate*, which was observed several times. Assuming that the initial number of cells plated was too high, which would affect the density and therefore possibly lead to the monolayer peeling off the plate, we reduced the initial number of cells plated, but this did not affect the peeling of the cells.

Shown in Figure 2A, the SVF cells obtained from the SubQ depot of both sexes differentiate to adipocytes in the presence of dox but not in its absence; this is because in (–) dox cell culture conditions, the dox activation of transgene h*AGPAT2* is lost, further confirming the role of AGPAT2 in differentiation of preadipocytes to adipocytes. It is also apparent upon ORO staining that compared with WT-SVF cell differentiation, the accumulation of neutral lipids in (+) dox Tg-$^{AT\text{-}hA2}$;m*A2*$^{-/-}$ SVF cells is less. As expected, the lipid accumulation of Tg-$^{AT\text{-}hA2}$;m*A2*$^{-/-}$ SVF in (–) dox conditions as shown by ORO staining was negligible (whole-well images of ORO staining are shown in Figure S5E).

We then amplified the h*AGPAT2* transcript expression in the presence or absence of dox (Figure 2B). As expected, those SVF cells cultured in (–) dox did not express h*AGPAT2* compared with those with (+) dox. We measured the expression of two key genes for early adipocyte differentiation, *Cebpα* and *Pparγ*; both increased in Tg-$^{AT\text{-}hA2}$;m*A2*$^{-/-}$ SVF cells cultured in the presence of dox compared with undifferentiated SVF cells. The mRNA expression of *Ap2*, a fatty-acid-binding protein, was also increased. Following this, we measured the expression of *Ucp1*, although this is a marker of BAT, to determine if the regenerated SubQ has acquired the molecular signature of beige adipocytes in cultured conditions. The expression of *Ucp1* did increases in the differentiated WT-SVF of SubQ of both sexes. *Ucp1* also increased in the differentiated (+) dox Tg-$^{AT\text{-}hA2}$;m*A2*$^{-/-}$ SVF cells of females but not males. However, *Ucp1* is not expressed in undifferentiated SVF cells (C_t > 30), so the fold changes in mature adipocytes (Avg C_t ~26) do not reflect a real fold change, but just an estimate. Even though *Ucp1* is a *bona fide* marker for BAT and beige AT, we note its expression even in our differentiated WT-SVF cells as well. Even though the role of *Ucp2* is not well defined in thermogenesis, we measured the expression of *Ucp2*, which increased ~2-fold in both differentiated WT-SVF cells and (+) dox Tg-$^{AT\text{-}hA2}$;m*A2*$^{-/-}$ SVF cells.

The differentiation of SVF cells obtained from BAT of both sexes also followed the pattern observed with SVF cells from SubQ. Shown in Figure 2C, the SVF cells obtained from the BAT depots of both sexes differentiate to adipocytes in the presence of dox but not in its absence. The accumulation of neutral lipids in (+) dox Tg-$^{AT\text{-}hA2}$;m*A2*$^{-/-}$ SVF cells is far less pronounced than in WT-SVF cells upon ORO staining (whole well images of ORO staining are shown in Figure S5F).

Similar to SubQ SVF cells, the BAT SVF cells kept in (–) dox did not express hAGPAT2 compared with those with (+) dox (Figure 2D). *Cebpα*, *Pparγ*, and *Ap2* all increased in Tg-$^{AT\text{-}hA2}$;m*A2*$^{-/-}$ SVF cells cultured in the presence of dox compared with undifferentiated SVF cells. Similar to SubQ SVF cells, *Ucp1* is not expressed in undifferentiated BAT SVF cells (C_t>30) but is expressed in differentiated BAT SVF cells of both sexes, so the fold changes in mature adipocytes (Avg C_t ~23) do not reflect a real fold change but just an estimate. *Ucp2* expression increased ~2- to 7-fold in both differentiated WT-SVF cells and (+) dox Tg-$^{AT\text{-}hA2}$;m*A2*$^{-/-}$ SVF cells of both sexes.

Turning off hAGPAT2 expression in adipose tissue in Tg-$^{AT\text{-}hA2}$;mA2$^{-/-}$ mice results in decreased adipose tissue and triacylglycerol content

As mentioned earlier, the lack of m*Agpat2* and loss of AT in *Agpat2*$^{-/-}$ mice precluded us from studying in any detail the role of this enzyme in AT. To accomplish this goal, we first regenerated the AT by turning on h*AGPAT2* under the adiponectin/Tet-O/CMV promoter by feeding doxycycline until 12 weeks of age. Subsequently, we turned off expression of h*AGPAT2* in AT by replacing the dox diet with the regular chow diet. Mice were euthanized at 4, 8, and 12 weeks after dox food removal, and the AT was collected for further examination (strategy is shown in Figure 3A).

As shown in Figure 3, turning off the expression of h*AGPAT2* resulted in a progressive decrease in the weight of the three AT depots studied for both sexes, anywhere from 44% to 100% depending upon the duration of removal of dox food (Figures 3B–3G), so much so that by 12 weeks of dox removal, almost no AT could be observed. Because chow-fed Tg-$^{AT\text{-}hA2}$;m*A2*$^{-/-}$ mice have no AT, no data are presented.

We biochemically measured the total TAG content of SubQ tissue from chow-fed WT and dox-fed Tg-$^{AT\text{-}hA2}$;m*A2*$^{-/-}$ mice at 12 weeks of dox feeding and 4 and 8 weeks of dox removal (Figures 3H and 3I). We could not measure the TAG content at 12 weeks of dox removal

CellPress
OPEN ACCESS

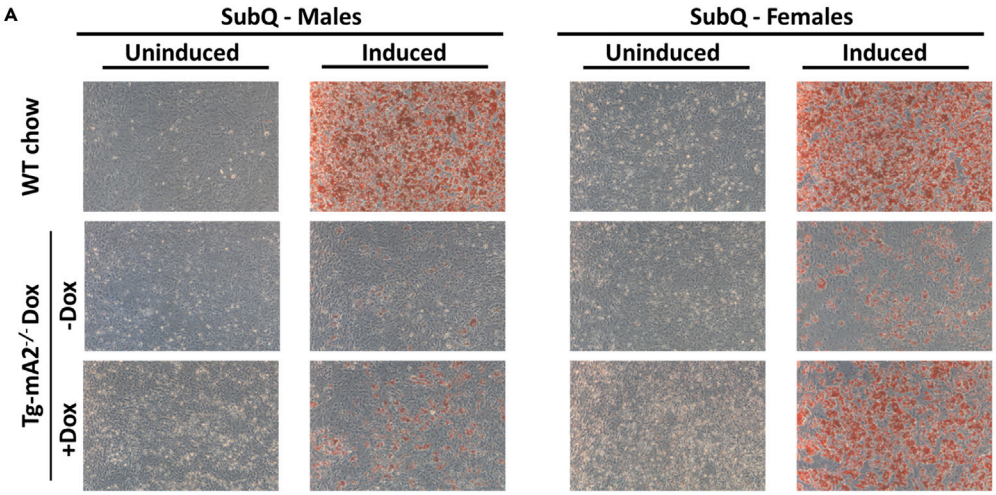

B

				hAgpat2		Cebpα		Pparγ		Ap2		Ucp1		Ucp2	
Genotype	Diet	Sex	in media	Uninduced	Induced	Uninduced	Induced	Uninduced	Induced	Uninduced	Induced	Uninduced	Induced	Uninduced	Induced
WT	chow	male	-dox	1.00	0.63 ± 0.35	1.00	11.12 ± 3.91	1.00	23.29 ± 7.42	1.00	394.17 ± 223.25	**1.00**	425.55 ± 441.41	1.00	2.12 ± 1.48
Tg-mA2$^{-/-}$	Dox	male	-dox	1.00	0.65 ± 0.11	1.00	3.39 ± 2.81	1.00	8.56 ± 7.03	1.00	505.34 ± 671.90	**1.00**	**0.95 ± 0.90**	1.00	1.18 ± 0.96
Tg-mA2$^{-/-}$	Dox	male	+dox	1.00	903.64 ± 1252.42	1.00	7.71 ± 7.81	1.00	13.88 ± 8.42	1.00	398.99 ± 381.29	**1.00**	**5.43 ± 3.11**	1.00	2.66 ± 3.56
WT	chow	female	-dox	1.00	0.39 ± 0.37	1.00	10.06 ± 10.40	1.00	33.71 ± 30.45	1.00	1080.62 ± 1440.25	**1.00**	432.76 ± 435.71	1.00	3.04 ± 4.68
Tg-mA2$^{-/-}$	Dox	female	-dox	1.00	0.49 ± 0.50	1.00	2.58 ± 1.88	1.00	5.73 ± 4.86	1.00	282.48 ± 224.04	**1.00**	**1.02 ± 1.36**	1.00	0.94 ± 1.22
Tg-mA2$^{-/-}$	Dox	female	+dox	1.00	616.72 ± 613.69	1.00	6.72 ± 5.41	1.00	17.21 ± 18.28	1.00	539.98 ± 630.27	**1.00**	46.56 ± 76.31	1.00	2.04 ± 2.62

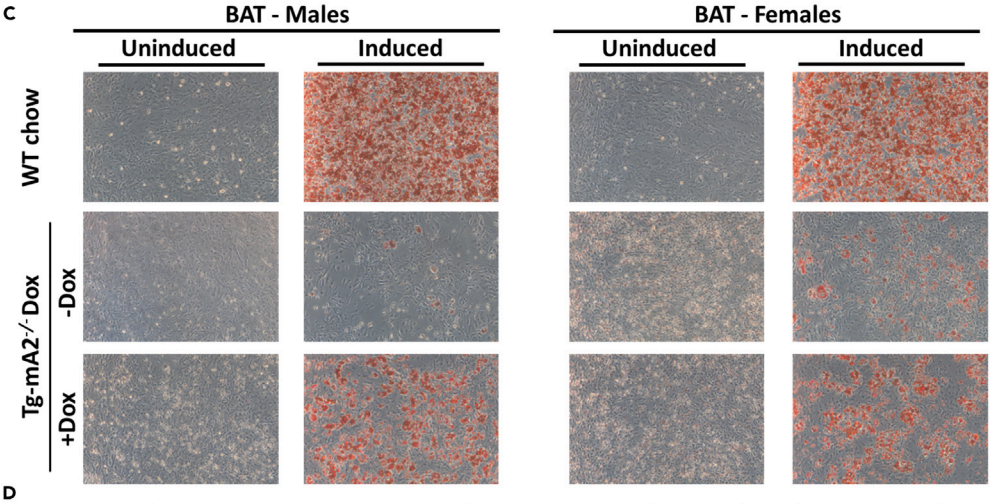

D

				hAgpat2		Cebpα		Pparγ		Ap2		Ucp1		Ucp2	
Genotype	Diet	Sex	in media	Uninduced	Induced	Uninduced	Induced	Uninduced	Induced	Uninduced	Induced	Uninduced	Induced	Uninduced	Induced
WT	chow	male	-dox	1.00	0.78 ± 0.24	1.00	13.79 ± 5.31	1.00	30.93 ± 16.19	1.00	528.75 ± 291.85	**1.00**	5129.32 ± 4392.19	1.00	6.98 ± 7.44
Tg-mA2$^{-/-}$	Dox	male	-dox	1.00	0.80 ± 0.17	1.00	1.67 ± 0.29	1.00	3.02 ± 1.50	1.00	70.17 ± 42.67	**1.00**	**1.09 ± 1.00**	1.00	2.64 ± 2.47
Tg-mA2$^{-/-}$	Dox	male	+dox	1.00	595.43 ± 367.72	1.00	5.91 ± 3.43	1.00	11.60 ± 5.83	1.00	344.03 ± 189.39	**1.00**	**486.70 ± 558.91**	1.00	2.55 ± 2.69
WT	chow	female	-dox	1.00	0.50 ± 0.31	1.00	17.02 ± 9.93	1.00	26.23 ± 19.10	1.00	1041.99 ± 694.96	**1.00**	4786.11 ± 3138.44	1.00	3.96 ± 2.40
Tg-mA2$^{-/-}$	Dox	female	-dox	1.00	0.75 ± 0.20	1.00	3.14 ± 2.08	1.00	6.09 ± 5.41	1.00	233.84 ± 156.38	**1.00**	**1.19 ± 0.72**	1.00	1.26 ± 0.34
Tg-mA2$^{-/-}$	Dox	female	+dox	1.00	511.53 ± 277.45	1.00	7.12 ± 3.43	1.00	11.07 ± 2.21	1.00	332.23 ± 142.09	**1.00**	1053.15 ± 1462.40	1.00	1.97 ± 0.21

Figure 2. *Ex vivo* induction of stromal vascular fraction (SVF) cells obtained from the dox-fed Tg-$^{AT\text{-}hA2}$;*mA2*$^{-/-}$ mice shows increased differentiation to adipocytes

SVF cells from subcutaneous (SubQ) and brown adipose tissue (BAT) from dox-fed Tg-$^{AT\text{-}hA2}$;*mA2*$^{-/-}$ mice, both male and female, were induced for adipocyte differentiation in the absence or presence of doxycycline (dox) in the culture media. SVF cells from chow-fed WT mice were grown and induced in the absence of dox.

(A) The representative 10x images of the undifferentiated and differentiated SubQ cells stained with the neutral lipid stain Oil Red O (ORO). Note that when dox is omitted from the culture media of Tg-$^{AT\text{-}hA2}$;*mA2*$^{-/-}$ cells, SVF do not differentiate.

(B) The RT-qPCR for select gene expression for adipogenesis on day 8 of differentiation in SubQ SVF cells. Note that the expression of h*AGPAT2* in Tg-$^{AT\text{-}hA2}$;*mA2*$^{-/-}$ SVF cells in the presence of dox is upregulated ~900-fold for males and ~600-fold for female.

(C) The representative 10x images of the undifferentiated and differentiated BAT cells stained with the neutral lipid stain Oil Red O (ORO). Note that when dox is omitted from the culture media of Tg-$^{AT\text{-}hA2}$;*mA2*$^{-/-}$ cells, SVF do not differentiate.

(D) The RT-qPCR for select gene expression for adipogenesis on day 8 of differentiation in BAT SVF cells. Note that the expression of h*AGPAT2* in Tg-$^{AT\text{-}hA2}$;*mA2*$^{-/-}$ SVF cells in the presence of dox is upregulated ~600-fold for male and ~510-fold for female. Fold changes in B and D are presented as mean ± SD (n = 3). Bold highlight indicates a C_t value over 30 (unexpressed). For full gene names, see STAR methods section Table S1. Tg-$^{AT\text{-}hA2}$;*mA2*$^{-/-}$ is abbreviated to Tg-m*A2*$^{-/-}$. See also Figure S5.

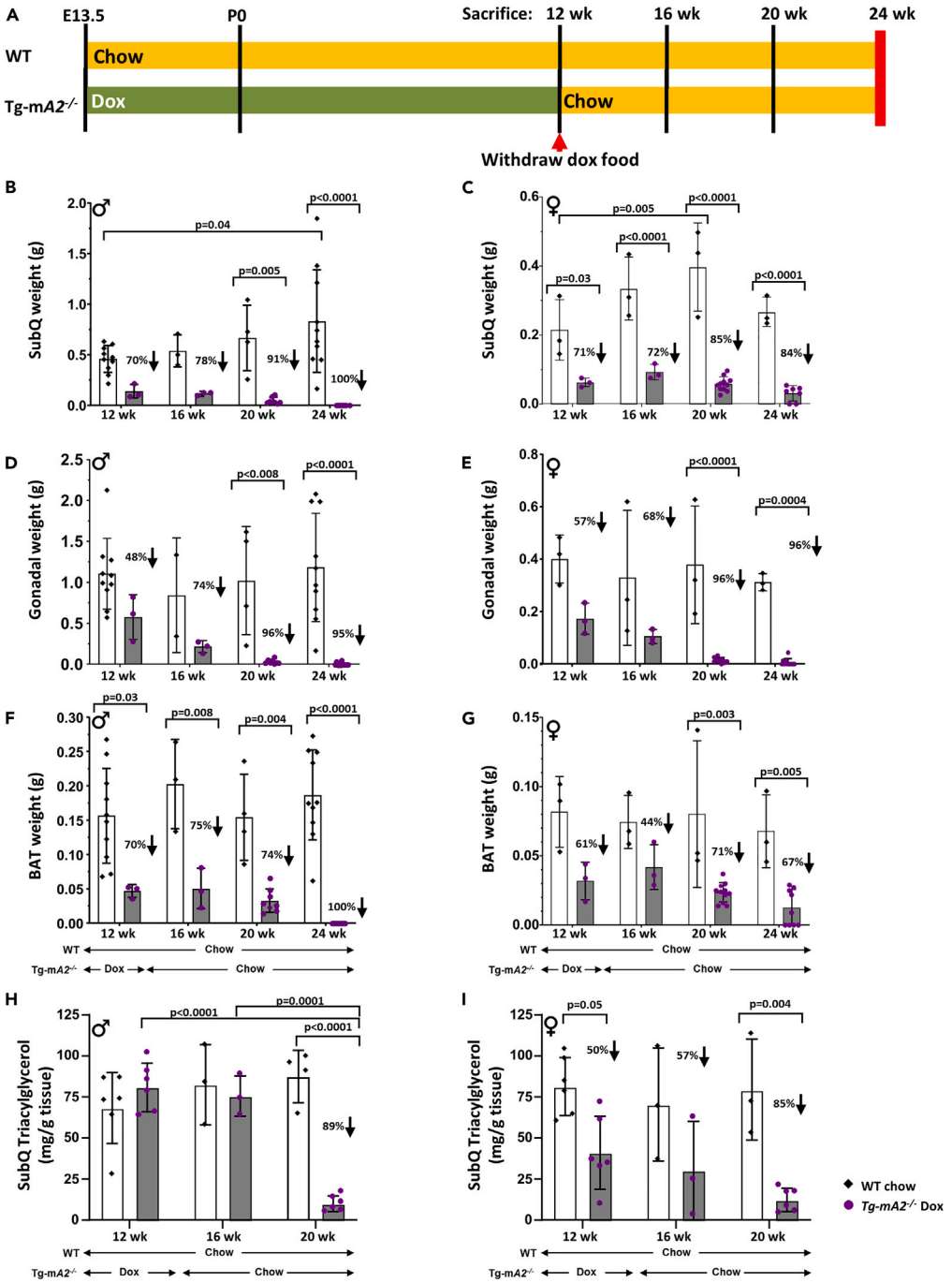

Figure 3. Weight of adipose tissue depots decreases upon turning off the expression of h*AGPAT2* in doxycycline (dox)-fed Tg-$^{AT\text{-}hA2}$;*mA2*$^{-/-}$ mice

(A) The strategy for feeding WT and dox-fed Tg-$^{AT\text{-}hA2}$;*mA2*$^{-/-}$ mice with subsequent dox-food removal (to turn off h*AGPAT2* expression).

(B–G) The adipose tissue weight of (B and C) subcutaneous (SubQ), (D and E) gonadal, and (F and G) brown adipose tissue (BAT) depots upon turning off expression of h*AGPAT2* for 4, 8, and 12 weeks after 12 weeks of dox feeding. There is a reduction in the adipose tissue in the three depots examined. This decrease is more prominent at 8 weeks after dox removal, and the adipose tissue is visually undetectable by 12 weeks of dox removal. Because SubQ tissue is slightly diffuse compared with gonadal fat, the true tissue weight could be slightly more than what we have weighed, but these are still relative tissue weights.

(H–I) Triacylglycerol (TAG) levels in SubQ adipose tissue. As the expression of hAGPAT2 is turned off, the TAG levels in the SubQ adipose tissue are reduced. The lines and arrows below panes (F-I) represent the chow and dox diet feeding strategy in mice. Each dot represents a different mouse; n = 3–12 mice in each group. Percentage decrease of Tg-$^{AT\text{-}hA2}$;*mA2*$^{-/-}$ mice compared with chow-fed WT mice at each time point is shown. The data are represented as mean ± SD. Tg-$^{AT\text{-}hA2}$;*mA2*$^{-/-}$ is abbreviated to Tg-*mA2*$^{-/-}$; p values are shown on the graph, determined using two-way ANOVA. The symbols ♂ (male) and ♀ (female) are embedded in the panels.

because there was almost no SubQ tissue to collect at this time point in the Tg-$^{AT\text{-}hA2}$;mA2$^{-/-}$ mice. We chose the SubQ tissue because this depot is known to synthesize and store TAG. We do note a progressive decrease in TAG content in SubQ tissue but it is more prominent in female SubQ than in male SubQ by 4 weeks of dox removal (57% decrease). The longer the h*AGPAT2* expression is turned off (up to 8 weeks), the more striking the decrease in TAG is. In this experiment, there are two events happening simultaneously: first, there seems to be less adipocyte differentiation and therefore less AT, and second, the reduction in AT reduces the synthesis of TAG and its storage.

Phospholipid and neutral lipid analysis in adipose tissue depots in male dox-fed and dox-removal in Tg-$^{AT\text{-}hA2}$;mA2$^{-/-}$ mice using lipid mass spectrometry approach

Profiling lipids in either patients with CGL1 (*AGPAT2* variants) or in *Agpat2*$^{-/-}$ null mice is impossible because both lack visible AT, therefore precluding us from measuring lipids. With our current mouse model, it now becomes possible to measure lipids in AT, both when the AT is regenerated and when the expression of h*AGPAT2* is turned off. This strategy allows us to determine whether there are changes in the lipid profile in the presence and absence of h*AGPAT2*. Because there is almost no AT visible by 12 weeks of dox food removal (as seen in Figure 3), we proceeded with lipidomics analysis from adipose depots harvested after 8 weeks of dox food removal, when there was still enough AT present for analysis.

The targeted lipid analysis for phospholipids and neutral lipids is presented in Figure S6. A comparison of dox-fed Tg-$^{AT\text{-}hA2}$;mA2$^{-/-}$ male mice compared with those when dox food was withdrawn for 8 weeks shows inconsistency in the phospholipid profiles between the AT depots, although we were not expecting such wide variations. We did not observe any significant changes in the levels of LPC, PC, LPE, PE, and PI. In general, PA is ~1%–3% of the phospholipids in tissues[36]; therefore, measuring its presence in tissues is very challenging, even more so in AT. In addition, we could detect LPA in our samples using the current extraction/detection method. Despite the fact that h*AGPAT2* is not expressed after 8 weeks of food removal, we observed a significant increase in PA levels in gonadal AT but not in SubQ and BAT; this is similar to what we observed in the livers of *Agapt2*$^{-/-}$ mice.[37] PI, a molecule involved in several signaling pathways, including insulin signaling, increased slightly in SubQ and gonadal AT, although not statistically significant, and decreased in BAT. Phosphatidylglycerol (PG) increased in SubQ and gonadal AT but not in BAT; the role of this lipid subclass is not well characterized in AT. The role each of these lipids plays in adipocytes is still unknown.

Upon removal of h*AGPAT2* expression (dox removal), there was a decrease in the neutral lipids DAG and TAG in the SubQ depot compared with dox-fed Tg-$^{AT\text{-}hA2}$;mA2$^{-/-}$ mice. However, they increased in gonadal AT while DAG increased in BAT but TAG decreased. BAT is most known for oxidative phosphorylation/ATP production and is not known to store TAG, other than for its usage in fatty acid oxidation. Why the ceramide levels increased in SubQ and gonadal depots but did not change in BAT remains unknown.

We then searched for specific molecular species of these lipid classes (Table 5). Here again, no specific pattern in the molecular species of phospholipid emerged among the three depots. For example, PA 34:0 increased 5.8-fold in SubQ but not in gonadal or BAT. On the other hand, three PA species (PA [36:2](18:0_18:2), PA [36:2](18:2_18:0), and PA [38:4](18:0_20:4)) were increased in gonadal AT but not in SubQ or BAT. We did not see any change in PA species in BAT. PG 38:6 (18:2_20:4) is increased 13- and 7-fold in SubQ and gonadal AT, respectively, in Tg-$^{AT\text{-}hA2}$;mA2$^{-/-}$ (dox removed) mice compared with dox-fed Tg-$^{AT\text{-}hA2}$;mA2$^{-/-}$ mice but not in BAT. PG 34:1(18:1_16:0) was increased modestly in SubQ but not in gonadal or BAT. PG is also a substrate for cardiolipin (CL) synthesis, a critical mitochondrial lipid essential for oxidative phosphorylation; elevated levels of PG is akin to Barth syndrome,[38] a mitochondrial CL defect. PG as a lipid mediator can favor WAT lipid storage.[39] Nevertheless, the functional role of PGs in AT is poorly characterized and requires further studies. Similar to phospholipids, neutral lipids such as DAG and TAG show more variation in SubQ and gonadal WAT but no change in BAT. Several molecular species of TAG were significantly altered between Tg-$^{AT\text{-}hA2}$;mA2$^{-/-}$ (dox removal) mice compared with dox-fed Tg-$^{AT\text{-}hA2}$;mA2$^{-/-}$ mice but only in SubQ AT. Two species, TAG 54:3 (18:1) and TAG 54:4 (18:1), were significantly increased in gonadal AT from Tg-$^{AT\text{-}hA2}$;mA2$^{-/-}$ (dox removal) mice compared with dox-fed Tg-$^{AT\text{-}hA2}$;mA2$^{-/-}$ mice but were decreased in the SubQ AT. No TAG species were significantly changed in BAT, although this is expected because BAT does not store TAG. Ceramide [42:2](d18:1_24:1) was increased in SubQ and gonadal WAT of Tg-$^{AT\text{-}hA2}$;mA2$^{-/-}$ (dox removal) mice compared with dox-fed Tg-$^{AT\text{-}hA2}$;mA2$^{-/-}$ mice but not in BAT. Other statistically significant differences between phospholipids in AT are shown in Table 5.

Phospholipid and neutral lipid analysis in adipose tissue depots in chow-fed WT and dox-fed Tg-$^{AT\text{-}hA2}$;mA2$^{-/-}$ mice using lipid mass spectrometry approach

We also compared chow-fed WT with dox-fed Tg-$^{AT\text{-}hA2}$;mA2$^{-/-}$ mice (Figure S6) to ascertain how much the levels of phospholipids and neutral lipids in regenerated AT normalized to WT mice. In general, we found no statistically significant difference between the two groups, as expected. However, LPC 18:1, PC 34:2 (18:2_16:0), PC 34:1 (18:1_16:0), and PA 36:2 (18:2_18:0) were all significantly decreased in dox-fed Tg-$^{AT\text{-}hA2}$;mA2$^{-/-}$ mice compared with chow-fed WT mice in BAT.

A search for a possible mechanism for decrease in adipose tissue upon turning off hAGPAT2 expression in Tg-$^{AT\text{-}hA2}$;mA2$^{-/-}$ mice

Upon turning off the expression of h*AGPAT2* (by dox food removal), the Tg-$^{AT\text{-}hA2}$;mA2$^{-/-}$ mice lose AT. The decrease in AT could be due to multiple reasons, for example, reduced hyperplasia, reduced repair of the plasma membrane, apoptosis, autophagy, necrosis, and in rare occasions, might also be due to mitotic catastrophe, reviewed in.[40,41] A few of these pathways, such as ferroptosis, require external

Table 5. Molecular species for phospholipid and neutral lipids are significantly altered between male chow-fed WT, doxycycline (dox)-fed Tg-$^{AT\text{-}hA2}$;mA2$^{-/-}$ mice, and dox-fed Tg-$^{AT\text{-}hA2}$;mA2$^{-/-}$ mice followed by 8 weeks dox removal

	SubQ		Gonadal		BAT	
	Fold Change		Fold Change		Fold Change	
	WT (=1) versus Tg-mA2$^{-/-}$ dox	Tg-mA2$^{-/-}$ dox (=1) versus Tg-mA2$^{-/-}$ dox removal	WT (=1) versus Tg-mA2$^{-/-}$ dox	Tg-mA2$^{-/-}$ dox (=1) versus Tg-mA2$^{-/-}$ dox removal	WT (=1) versus Tg-mA2$^{-/-}$ dox	Tg-mA2$^{-/-}$ dox (=1) versus Tg-mA2$^{-/-}$ dox removal
Phospholipids						
LPC 18:1	—	—	—	1.78[a]	0.39[c]	—
PC (18:2_16:0)	—	—	—	—	0.57[a]	—
PC (18:1_16:0)	—	—	—	—	0.55[a]	—
PC (18:2_18:0)	—	0.31[a]	—	—	—	0.51[b]
LPE 18:0	—	—	—	—	—	0.68[a]
LPE 18:1	—	2.22[a]	—	—	—	—
PA (16:0_18:0)	—	5.77[c]	—	—	—	—
PA (18:2_18:0)	—	—	—	—	0.48[a]	—
PA (18:0_18:2)	—	—	—	3.72[b]	—	—
PA (18:2_18:0)	—	—	—	3.77[a]	—	—
PA (18:0_20:4)	—	—	—	2.22[c]	—	—
PI (18:0_20:4)	—	—	—	2.01[a]	—	0.38[a]
PG (18:1_16:0)	—	2.34[a]	—	—	—	—
PG (18:2_20:4)	—	13.32[a]	—	7.05[c]	—	—
Neutral Lipids						
DAG (18:1_18:1)	—	0.17[c]	—	2.05[a]	—	5.18[c]
DAG (18:2_18:1)	—	0.16[a]	—	—	—	—
DAG (18:1_18:2)	—	0.13[a]	—	—	—	—
DAG (18:2_16:0)	—	0.05[a]	—	—	—	—
TAG 54:3	—	0.54[a]	—	5.06[c]	2.77[a]	—
TAG 54:4	—	—	—	4.27[a]	—	—
Cer (d18:1/24:1)	—	4.00[c]	—	3.35[c]	—	—
Cer (d18:1/22:0)	—	—	—	—	—	0.36[a]

Shown are the fold changes for species that are significantly different between the two groups shown. n = 3. SubQ, subcutaneous; BAT, brown adipose tissue. Statistics were determined by two-way ANOVA. Tg-$^{AT\text{-}hA2}$;mA2$^{+/+}$ is abbreviated to WT. Tg-$^{AT\text{-}hA2}$;mA2$^{-/-}$ is abbreviated to Tg-mA2$^{-/-}$. See also Figure S6.

[a]$p < 0.05$,

[b]$p < 0.001$,

[c]$p < 0.0001$.

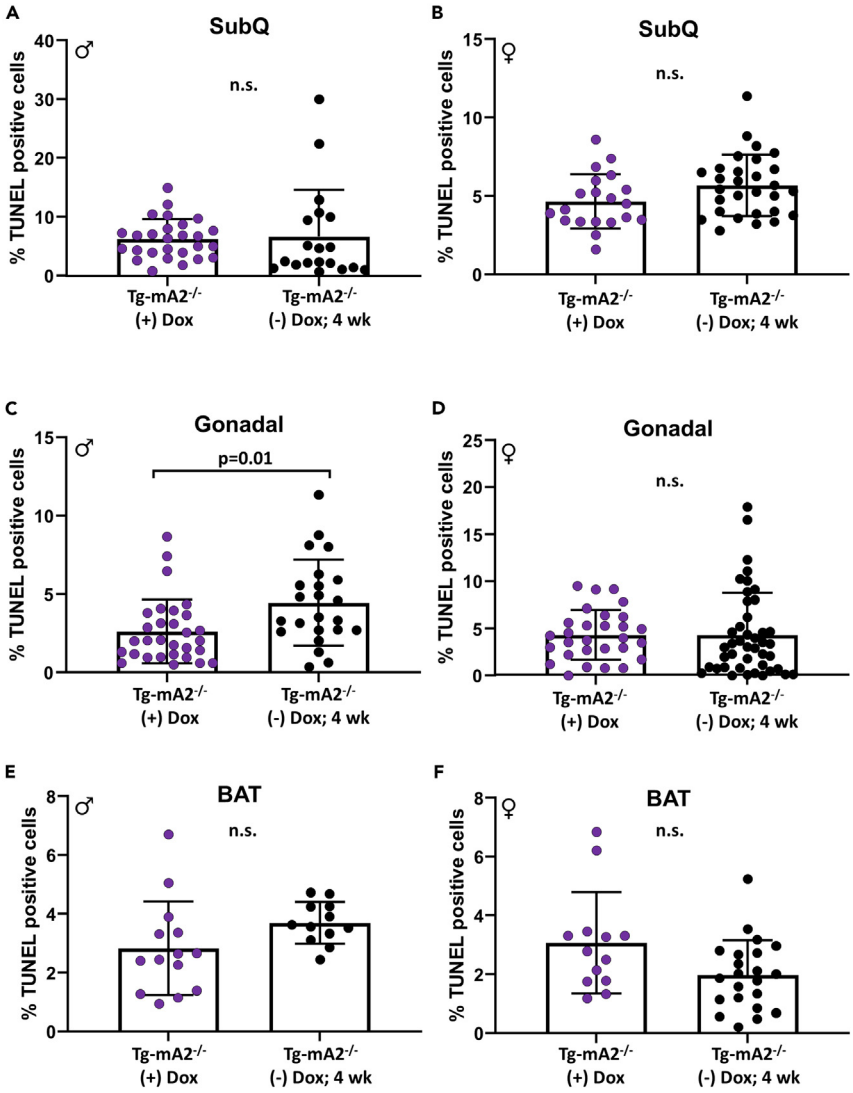

Figure 4. Adipose tissue cell death (apoptosis) assessed by TUNEL method

(A and B) The percent positive nuclei in (A) male and (B) female subcutaneous (SubQ) adipose tissue.

(C and D) The percent positive nuclei in (C) male and (D) female gonadal adipose tissue.

(E and F) The percent positive nuclei in (E) male and (F) female brown adipose tissue (BAT). Adipose tissue was obtained from Tg-$^{AT\text{-}hA2}$;m*A2*$^{-/-}$ mice fed dox food for 12 weeks and Tg-$^{AT\text{-}hA2}$;m*A2*$^{-/-}$ mice fed doxycycline (dox) food for 12 weeks followed by 4 weeks of dox removal (to turn off h*AGPAT2* expression). Each dot represents an individual field of counted cells. Tissue from 2 to 3 mice for each group was collected, and 9–17 fields per tissue were examined. The data are represented as mean ± SD; p values are shown on the graph, determined using mixed model repeated measurements. ns = nonsignificant. Tg-$^{AT\text{-}hA2}$;m*A2*$^{-/-}$ is abbreviated to Tg-m*A2*$^{-/-}$. The symbols ♂ (male) and ♀ (female) are embedded in the panels.

factor(s); others, such as apoptosis, are usually initiated intracellularly. In ferroptosis, cell death requires iron-driven oxidized phospholipids.[42] Autophagy can be initiated by either internal or external factors. In this study, we focused on a more common cause of cell death: apoptosis.

Using terminal deoxynucleotidyl transferase (TdT) dUTP Nick-End Labeling (TUNEL) methods, we studied the cell death in WAT (SubQ and gonadal) and BAT of both sexes. As shown in Figures 4A and 4B, in SubQ AT of both sexes, the number of apoptotic cells detected was no different whether the expression of h*AGPAT2* was turned on or off. However, we did observe a statistically significant increase in apoptotic cells in male gonadal AT (Figure 4C) but not in females (Figure 4D). The apoptotic levels were similar in the BAT as in the gonadal AT (Figures 4E and 4F) but did not reach statistical significance. Because one of the pathways for generation of phospholipids is knocked out, we expected that cell death should have been similar in both the AT depots of both sexes. Our observation suggests that apoptosis is most likely not the main cause of reduced AT and requires additional focused studies related to cellular death/reduction in the AT.

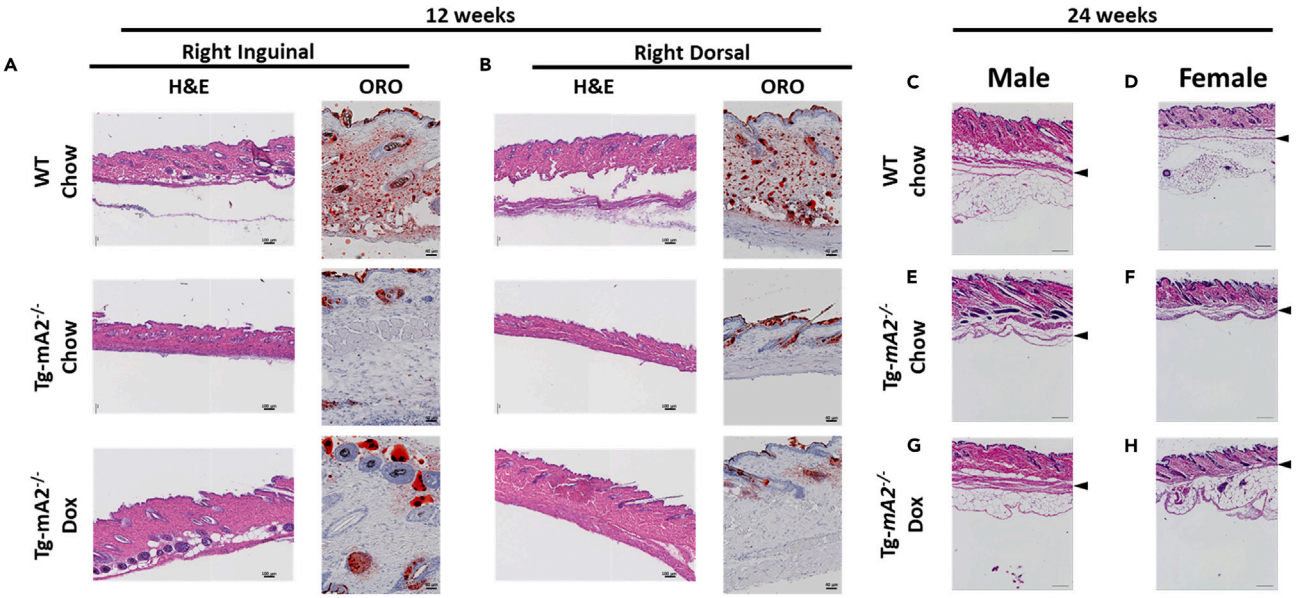

Figure 5. Skin from doxycycline (dox)-fed Tg-$^{AT\text{-}hA2}$;m*A2*$^{-/-}$ mice shows regeneration of dermal white adipose tissue (dWAT)

(A and B) Representative images of skin from the (A) right inguinal and (B) right dorsal of 12 weeks male chow-fed WT, chow-fed Tg-$^{AT\text{-}hA2}$;m*A2*$^{-/-}$, and dox-fed Tg-$^{AT\text{-}hA2}$;m*A2*$^{-/-}$ mice. Cryopreserved skin sections were stained with H&E or Oil Red O (ORO) and counterstained with H&E. The dWAT can be appreciated in the WT mice, both in the H&E and ORO sections but not in chow-fed Tg-$^{AT\text{-}hA2}$;m*A2*$^{-/-}$ mice. Upon turning on the expression of hAGPAT2 for 12 weeks, there is a hint of regeneration of dWAT. The clear adipocyte layer is not visible due to artifacts of cryosectioning. Scale bars for 12 weeks H&E are 100 μm. Scale bars for 12 weeks ORO are 40 μm.Tg-$^{AT\text{-}hA2}$;m*A2*$^{-/-}$ is abbreviated to Tg-m*A2*$^{-/-}$.

(C–H) Representative images of dorsal skin from 24 weeks (C and D) chow-fed WT, (E and F) chow-fed Tg-$^{AT\text{-}hA2}$;m*A2*$^{-/-}$, and (G and H) dox-fed Tg-$^{AT\text{-}hA2}$;m*A2*$^{-/-}$ mice of both sexes that were fixed in paraformaldehyde and stained with H&E. Re-expression of hAGPAT2 for 24 weeks results in much greater regeneration of dWAT than was seen at 12 weeks. Black arrowheads indicate the panniculus carnosus. Scale bars for 24 weeks H&E are 200 μm. Tg-$^{AT\text{-}hA2}$;m*A2*$^{-/-}$ is abbreviated to Tg-m*A2*$^{-/-}$. See also Figures S7A–S7C.

Partial regeneration of dermal white adipose tissue (dWAT) in dox-fed Tg-$^{AT\text{-}hA2}$;mA2$^{-/-}$ mice

In general, the AT (adipocytes) beneath the skin is referred to as subcutaneous AT. However, distinct adipocyte depots exist in the skin where several layers of adipocytes lie adjacent to the epidermis (Figure S7A).[43] In mice (rodents), this layer of adipocytes exists as two layers separated by striated muscle, the panniculus carnosus.[44] In humans, this separation is lost. The adipocytes directly beneath the epidermis and above the panniculus carnosus in mice are defined as dermal WAT (dWAT).

The skin of the *Agpat2*$^{-/-}$ mice is very thin compared with WT mice of both sexes. We histologically studied the skin from male chow-fed and dox-fed Tg-$^{AT\text{-}hA2}$;m*A2*$^{-/-}$ mice for the absence or regeneration of dWAT (Figure 5). At 12 weeks, the skin from the right inguinal and right dorsal region was excised and cryopreserved (Figures 5A and 5B). The tissue sections were stained for ORO (presence of lipid) and counterstained with H&E. Right dorsal skin sections from chow-fed WT mice show a space beneath the epidermis, but above the panniculus carnosus, suggesting the presence of adipocytes, dWAT, although not visible due to cryosectioning. Chow-fed Tg-$^{AT\text{-}hA2}$;m*A2*$^{-/-}$ mice have no such space (region) and lack dWAT; the epidermis is tightly juxtaposed with the panniculus carnosus. The skin of the dox-fed Tg-$^{AT\text{-}hA2}$;m*A2*$^{-/-}$ mice appears to be similar to chow-fed Tg-$^{AT\text{-}hA2}$;m*A2*$^{-/-}$ mice except that it is slightly thicker, although we do not observe a space where the dWAT would be localized. It may be that 12 weeks is not enough time to regenerate the dWAT in the dermal region. When the cryopreserved skin sections were stained for lipids (by ORO staining), while we note the ORO staining of lipid droplets in the WT mice, both chow-fed and dox-fed Tg-$^{AT\text{-}hA2}$;m*A2*$^{-/-}$ mice have only a few droplets that are associated with the hair follicle. This feature is more clear in the skin obtained from the right inguinal region of the mouse, where the WT mice have substantial ORO staining, whereas there is moderate ORO staining in dox-fed Tg-$^{AT\text{-}hA2}$;m*A2*$^{-/-}$ mice. This observation would suggest the presence of dWAT beneath the skin is uneven; some anatomical regions have more adipocytes than the other regions.

We extended this observation in 24-week-old male mice and included female mice as well. At 24 weeks, the skin from only the dorsal region was studied. The skin was excised, fixed in paraformaldehyde, and tissue sections stained with H&E. In our hands, the ORO staining in cryopreserved sections was not impressive, so we only performed paraffin-embedded sections with H&E staining. At this mouse age, there is further increase in the dWAT in the WT mouse (Figures 5C and 5D), whereas in chow-fed Tg-$^{AT\text{-}hA2}$;m*A2*$^{-/-}$ mice dWAT is essentially undetectable (Figures 5E and 5F). In the dox-fed Tg-$^{AT\text{-}hA2}$;m*A2*$^{-/-}$ mice, while SubQ adipocytes (below the panniculus carnosus) are significantly increased, the presence of dWAT still remains unappreciable (Figures 5G and 5H). The whole skin images are shown in Figures S7B and S7C.

DISCUSSION

The current study shows that the embryonic expression of h*AGPAT2* driven by the adiponectin/Tet-O/CMV promoters regenerates the AT in all three major metabolically active depots (SubQ, Gonadal, and BAT), as well as dWAT (skin), in *Agpat2*$^{-/-}$ mice. Despite the expression of h*AGPAT2* from an embryonic stage well into adult life, the development of AT depots did not reach the same level (by weight) as those of age-matched WT mice; it remained ~30%–50% of the levels observed in WT mice for both sexes. This would suggest one of two things: either there is additional input of other organ systems that aid in the development of AT in adult life or there is specificity of promoter usage in different adipose depots. Here, the adiponectin/Tet-O/CMV promoter, not the endogenous promoter used by *Agpat2* for its expression in mice, drives the expression of h*AGPAT2*. In addition, endogenous AGPAT2 may be expressed earlier in adipocyte precursors, whereas adiponectin only turns on late in differentiation.

The origins of WAT and BAT in animals are of different cellular lineages.[45] The notion that AGPAT2 is involved in phospholipid and TAG synthesis and not so much in adipocyte lineage differentiation is contrary to this thinking. The role of AGPAT2 in BAT is not well established. Absence of AGPAT2 results in loss of BAT. Whether it has a dual role of cellular differentiation and TAG synthesis needs further investigations. If AGPAT2 were solely involved in TAG synthesis, the presence of BAT should not have been detectable. However, we did observe the regeneration of BAT, which further substantiates AGPAT2's involvement in adipocyte lineage determination for both WAT and BAT. Future studies related to adipocyte lineage analysis will confirm this observation.

In this study, we also demonstrate that when the expression of h*AGPAT2* is turned off (by dox food removal) for 4, 8, 12 weeks following 12 weeks of h*AGPAT2* expression, the regenerated AT begins to decrease, so much so that by 12 weeks of dox removal, the AT is almost undetectable. This decrease is observed in all three AT depots and in both sexes, which further supports the critical role of AGPAT2 in the development and maintenance of AT. Furthermore, when we isolated SVF cells from SubQ and BAT in 12 weeks WT and dox-fed **Tg-**$^{\text{AT-hA2}}$**;m*A2***$^{-/-}$ mice, and subjected them to *in vitro* differentiation to mature adipocytes, we noticed similar differentiation in SVF cells obtained from WT and dox-fed **Tg-**$^{\text{AT-hA2}}$**;m*A2***$^{-/-}$ AT. However, this differentiation of SVF cells from **Tg-**$^{\text{AT-hA2}}$**;m*A2***$^{-/-}$ mice required the presence of doxycycline in the culture media and therefore h*AGPAT2* expression. When absent, the cells failed to differentiate, indicating the importance of *Agpat2*'s role in adipocyte differentiation. The failure of **Tg-**$^{\text{AT-hA2}}$**;m*A2***$^{-/-}$ SVF cells to differentiate in the absence of doxycycline (and therefore without h*Agpat2* expression), even in the presence of rosiglitazone, a *Pparγ* agonist, clearly indicates that either *Agpat2* generates ligand(s) that cooperate with *Pparγ* to set in motion cellular differentiation or, alternatively, the function of *Agpat2* lies upstream of *Pparγ*. We also observed that despite the many fold increase in the expression of h*AGPAT2* (~1000-fold), the cellular differentiation was still less than those observed in the WT SVF cells. This observation again suggests that there are likely additional inputs still missing in the regenerated SVF cells that inhibit these SVF cells from achieving full potential for differentiation.

Because AGPAT2 acts upstream of *Pparγ*, and it synthesizes phospholipids, it is logical to assume that some phospholipid species are either not generated or the molecule species that are generated in its absence become inhibitory. The search for endogenous ligands for *Pparγ* has been ongoing, and a few of the ligands that activate *Pparγ*, such as long-chain free fatty acids such as arachidonic acid and its metabolites, 15-deoxy-$\Delta^{12,14}$-prostaglandin J_2,[46] and nonsteroidal anti-inflammatory drugs (NSAIDs),[47] have been shown to modulate *Pparγ* activity. *In silico* simulation studies show that LPC (C16, C18:0, C18:1, C18:2) have affinity toward *Pparγ*.[48] Although in our study LPC18:1 does not seem to be a ligand *in vivo*, additional phospholipids measured need to be tested individually or collectively in the differentiation of adipocyte precursors.

In a targeted lipid mass spectrometry analysis of phospholipids and neutral lipids in male AT depots in **Tg-**$^{\text{AT-hA2}}$**;m*A2***$^{-/-}$ mice fed doxycycline for 12 weeks compared with those mice where the dox food was removed for 8 weeks, there were no striking changes in total phospholipid content between these 2 groups. Nevertheless, there are a few differences in molecular lipid species. In general, there is an increase in phospholipids, mostly in WAT, whereas there is a decrease in DAG and TAG, as shown in Table 5. A decrease in WAT (tissue weight) and a reduction in SVF cell differentiation would suggest that increases in these lipid species are in fact going to be detrimental to cellular differentiation. We encountered some technical challenges regarding phospholipids extraction from AT with the acidified n-butanol solvent we usually used to extract the phospholipids PA and LPA[37] (the extract became "oily" and could not be used for LC-MS/MS). Therefore, we used $CHCl_3$:CH_3OH for the lipid extraction. The other challenge is that cellular PA is very low (~1%–3% of the total phospholipid content in yeast),[36] which becomes difficult to measure in the face of high levels of PC and PE. Additional extraction and MS analysis in WAT/BAT is required to measure extremely low levels of PA and LPA, as well as improved detection of additional molecular species of PA that could aid in the differentiation of adipocytes. Although unbiased lipidomics analysis did not reveal any statistically significant difference in TAG content, we did observe a decrease in TAG content by biochemical measurements. Future studies are required to adopt efficient lipid extraction to encompass all lipid classes and especially those that are represented in very low abundance and to create a "Lipid Map" for murine AT depots. A similar study has recently been reported for human AT.[49]

Not currently studied is the contribution of peroxisomal-acyl-DHAP pathway (Figure S7D) for the generation of ether lipids—lipids containing an oxygen atom connected to two alkyl or aryl groups. In fact, one study reports that almost 50% of total TAG arises from the above pathway ([50] and reviewed in[51,52]). In the current study, we measured TAG via a biochemical method that uses lipases to generate FFA and glycerol, which is then measured chemically. We also used mass spectroscopy because the biochemical method does not use alkylglycerol monooxygenase (AGMO), the only enzyme that can cleave the ether linkage (1-*O*-alkyl), and we may have therefore omitted estimating the ether-linked TAG. However, in our mass spectroscopy measurements, we did not target ether lipids and so do not present ester- versus ether-linked TAG.

A major function of dWAT is in hair development, hair maintenance,[53] and wound healing.[54,55] We did not note a substantial hair loss in our chow-fed **Tg-**$^{\text{AT-hA2}}$**;m*A2***$^{-/-}$ mice, suggesting that dWAT aids in maintaining the hair growth but is not essential for its development. The role

of dWAT in wound healing was not examined in chow-fed **Tg-$^{AT\text{-}hA2}$;mA2$^{-/-}$** mice and will be the focus for future studies. In this regard, this mouse model could be beneficial to studying localized scleroderma (LoS) and the role of dWAT in this process[56] or in the study of the pathophysiology of acne.

In summary, and for the first time, we showed the role of *Agpat2* in *in vivo* AT generation and adipocyte differentiation but less of a role in TAG synthesis; this substantiates the notion that *Agpat2*'s role is more involved in adipocyte commitment and differentiation than in TAG synthesis. Interestingly, we also observed that dWAT is regenerated more slowly in relation to the other AT depots. We propose that this transgenic model will be very helpful in understanding the generation and expansion of AT in the animal's adult life and the study of skin-related diseases such as localized scleroderma (LoS), and the pathophysiology of acne. Although in the past mature adipocytes were permanently labeled to study adipogenesis,[57] the murine model described here will enable tracing of adipocyte lineage embryonically.

Limitations of the study

Limitations of the study include examining the generation of AT at only two time points in the animals. Longitudinal studies are needed to determine at which times of life the AT generation is initiated. A substantially smaller AT mass requires studies pertaining to the cell types that constitute the AT such as endothelial cells and cells of the immune system, including resident immune cells. In addition, *Agpat2* expression can be initiated before E13.5 in mice to determine cellular commitment toward preadipocytes.

STAR★METHODS

Detailed methods are provided in the online version of this paper and include the following:

- KEY RESOURCES TABLE
- RESOURCE AVAILABILITY
  - Lead contact
  - Materials availability
  - Data and code availability
- EXPERIMENTAL MODEL DETAILS
- METHOD DETAILS
  - Generation of transgenic AGPAT2 mouse model
  - Generation of h*AGPAT2* expression in m*Agpat2*$^{-/-}$ background
  - Mouse genotyping
  - Magnetic resonance imaging and spectrometry
  - Nuclear magnetic resonance
  - Differentiation of stromal vascular fraction (SVF) cells
  - Total RNA isolation
  - Reverse transcription quantitative polymerase chain reaction (RT-qPCR)
  - Quantitative PCR using pooled sample strategy
  - Triacylglycerol (TAG) assay
  - TUNEL assay
  - Lipid mass spectrometry
  - Tandem mass tag-mass spectrometry (TMT-MS) for adipose tissue
  - Peptide labeling and fractionation
  - Peptides mass spectrometry
  - Protein identification
  - Histological analysis
  - Plasma leptin measurements
- QUANTIFICATION AND STATISTICAL ANALYSIS

SUPPLEMENTAL INFORMATION

Supplemental information can be found online at https://doi.org/10.1016/j.isci.2023.107806.

ACKNOWLEDGMENTS

The authors thank Robert Hammer and members of the Transgenic Core for generation of the transgenic mouse model, the UTSW Proteomics Core for assistance with proteomics experiments, and John Shelton, along with the members of the histopathology core, for the staining of adipose tissue samples. Graphical abstract mouse image was obtained from Wikimedia Commons under a Creative Commons Attribution 4.0 International license (https://creativecommons.org/licenses/by/4.0/legalcode). Image modification: Graphics and text layered on top of the original image.

Funding and additional information: National Institutes of Health R01- DK105448, 1P30DK127984, R01-DK055758, R01-DK131537, UL1TR003163, and P01HL160487 and the Southwestern Medical Foundation supported this work. The content is solely the responsibility of the authors and does not necessarily represent the official views of the National Institutes of Health.

AUTHOR CONTRIBUTIONS

AKA designed, supervised, helped collect data, analyzed the data, and wrote the first draft. KT collected most of the data, prepared figures, and copyedited the manuscript. JGM and GV provided the lipidomic data. XL carried out additional statistical analysis. PES: resource and comments. JDH and AG reviewed the manuscript and provided comments. All authors reviewed and edited the manuscript.

DECLARATION OF INTERESTS

The authors declare no competing interests.

Received: February 21, 2023
Revised: June 28, 2023
Accepted: August 30, 2023
Published: September 1, 2023

REFERENCES

1. Agarwal, A.K., and Garg, A. (2006). Genetic basis of lipodystrophies and management of metabolic complications. Annu. Rev. Med. *57*, 297–311. https://doi.org/10.1146/annurev.med.57.022605.114424.
2. Agarwal, A.K., and Garg, A. (2006). Genetic disorders of adipose tissue development, differentiation, and death. Annu. Rev. Genom. Hum. Genet. *7*, 175–199. https://doi.org/10.1146/annurev.genom.7.080505.115715.
3. Foss-Freitas, M.C., Akinci, B., Luo, Y., Stratton, A., and Oral, E.A. (2020). Diagnostic strategies and clinical management of lipodystrophy. Expet Rev. Endocrinol. Metabol. *15*, 95–114. https://doi.org/10.1080/17446651.2020.1735360.
4. Agarwal, A.K., Arioglu, E., De Almeida, S., Akkoc, N., Taylor, S.I., Bowcock, A.M., Barnes, R.I., and Garg, A. (2002). AGPAT2 is mutated in congenital generalized lipodystrophy linked to chromosome 9q34. Nat. Genet. *31*, 21–23. https://doi.org/10.1038/ng880ng880.
5. Agarwal, A.K. (2012). Lysophospholipid acyltransferases: 1-acylglycerol-3-phosphate O-acyltransferases. From discovery to disease. Curr. Opin. Lipidol. *23*, 290–302. https://doi.org/10.1097/MOL.0b013e328354fcf4.
6. Agarwal, A.K., and Garg, A. (2003). Congenital generalized lipodystrophy: significance of triglyceride biosynthetic pathways. Trends Endocrinol. Metabol. *14*, 214–221.
7. Cortés, V.A., Curtis, D.E., Sukumaran, S., Shao, X., Parameswara, V., Rashid, S., Smith, A.R., Ren, J., Esser, V., Hammer, R.E., et al. (2009). Molecular mechanisms of hepatic steatosis and insulin resistance in the AGPAT2-deficient mouse model of congenital generalized lipodystrophy. Cell Metabol. *9*, 165–176. https://doi.org/10.1016/j.cmet.2009.01.002.
8. Cautivo, K.M., Lizama, C.O., Tapia, P.J., Agarwal, A.K., Garg, A., Horton, J.D., and Cortés, V.A. (2016). AGPAT2 is essential for postnatal development and maintenance of white and brown adipose tissue. Mol. Metabol. *5*, 491–505. https://doi.org/10.1016/j.molmet.2016.05.004.
9. González-Hódar, L., McDonald, J.G., Vale, G., Thompson, B.M., Figueroa, A.M., Tapia, P.J., Robledo, F., Agarwal, A.K., Garg, A., Horton, J.D., and Cortés, V. (2021). Decreased caveolae in AGPAT2 lacking adipocytes is independent of changes in cholesterol or sphingolipid levels: A whole cell and plasma membrane lipidomic analysis of adipogenesis. Biochim. Biophys. Acta, Mol. Basis Dis. *1867*, 166167. https://doi.org/10.1016/j.bbadis.2021.166167.
10. Tapia, P.J., Figueroa, A.M., Eisner, V., González-Hódar, L., Robledo, F., Agarwal, A.K., Garg, A., and Cortés, V. (2020). Absence of AGPAT2 impairs brown adipogenesis, increases IFN stimulated gene expression and alters mitochondrial morphology. Metabolism *111*, 154341. https://doi.org/10.1016/j.metabol.2020.154341.
11. Gale, S.E., Frolov, A., Han, X., Bickel, P.E., Cao, L., Bowcock, A., Schaffer, J.E., and Ory, D.S. (2006). A regulatory role for 1-acylglycerol-3-phosphate-O-acyltransferase 2 in adipocyte differentiation. J. Biol. Chem. *281*, 11082–11089. https://doi.org/10.1074/jbc.M509612200.
12. Subauste, A.R., Das, A.K., Li, X., Elliott, B.G., Evans, C., El Azzouny, M., Treutelaar, M., Oral, E., Leff, T., and Burant, C.F. (2012). Alterations in Lipid Signaling Underlie Lipodystrophy Secondary to AGPAT2 Mutations. Diabetes. db12-0004 *61*, 2922–2931. https://doi.org/10.2337/db12-0004.
13. Wang, Z.V., Deng, Y., Wang, Q.A., Sun, K., and Scherer, P.E. (2010). Identification and characterization of a promoter cassette conferring adipocyte-specific gene expression. Endocrinology *151*, 2933–2939. https://doi.org/10.1210/en.2010-0136.
14. Sun, K., Wernstedt Asterholm, I., Kusminski, C.M., Bueno, A.C., Wang, Z.V., Pollard, J.W., Brekken, R.A., and Scherer, P.E. (2012). Dichotomous effects of VEGF-A on adipose tissue dysfunction. Proc. Natl. Acad. Sci. USA *109*, 5874–5879. https://doi.org/10.1073/pnas.1200447109.
15. Fujimoto, N., Matsuo, N., Sumiyoshi, H., Yamaguchi, K., Saikawa, T., Yoshimatsu, H., and Yoshioka, H. (2005). Adiponectin is expressed in the brown adipose tissue and surrounding immature tissues in mouse embryos. Biochim. Biophys. Acta *1731*, 1–12. https://doi.org/10.1016/j.bbaexp.2005.06.013.
16. Qiao, L., Yoo, H.S., Madon, A., Kinney, B., Hay, W.W., Jr., and Shao, J. (2012). Adiponectin enhances mouse fetal fat deposition. Diabetes *61*, 3199–3207. https://doi.org/10.2337/db12-0055.
17. Hong, K.Y., Bae, H., Park, I., Park, D.Y., Kim, K.H., Kubota, Y., Cho, E.S., Kim, H., Adams, R.H., Yoo, O.J., and Koh, G.Y. (2015). Perilipin+ embryonic preadipocytes actively proliferate along growing vasculatures for adipose expansion. Development *142*, 2623–2632. https://doi.org/10.1242/dev.125336.
18. Das, K., Lin, Y., Widen, E., Zhang, Y., and Scherer, P.E. (2001). Chromosomal localization, expression pattern, and promoter analysis of the mouse gene encoding adipocyte-specific secretory protein Acrp30. Biochem. Biophys. Res. Commun. *280*, 1120–1129. https://doi.org/10.1006/bbrc.2001.4217.
19. Corbetta, S., Bulfamante, G., Cortelazzi, D., Barresi, V., Cetin, I., Mantovani, G., Bondioni, S., Beck-Peccoz, P., and Spada, A. (2005). Adiponectin expression in human fetal tissues during mid- and late gestation. J. Clin. Endocrinol. Metab. *90*, 2397–2402. https://doi.org/10.1210/jc.2004-1553.
20. Han, H., Qi, R., Zhou, J.J., Ta, A.P., Yang, B., Nakaoka, H.J., Seo, G., Guan, K.L., Luo, R., and Wang, W. (2018). Regulation of the Hippo Pathway by Phosphatidic Acid-Mediated Lipid-Protein Interaction. Mol. Cell *72*, 328–340.e8. https://doi.org/10.1016/j.molcel.2018.08.038.
21. Ardestani, A., Lupse, B., and Maedler, K. (2018). Hippo Signaling: Key Emerging Pathway in Cellular and Whole-Body Metabolism. Trends Endocrinol. Metabol. *29*, 492–509. https://doi.org/10.1016/j.tem.2018.04.006.
22. Ye, R.Z., Richard, G., Gévry, N., Tchernof, A., and Carpentier, A.C. (2022). Fat Cell Size: Measurement Methods, Pathophysiological Origins, and Relationships With Metabolic Dysregulations. Endocr. Rev. *43*, 35–60. https://doi.org/10.1210/endrev/bnab018.
23. Grabner, G.F., Xie, H., Schweiger, M., and Zechner, R. (2021). Lipolysis: cellular mechanisms for lipid mobilization from fat stores. Nat. Metab. *3*, 1445–1465. https://doi.org/10.1038/s42255-021-00493-6.
24. Takahashi, S., Sakai, J., Fujino, T., Hattori, H., Zenimaru, Y., Suzuki, J., Miyamori, I., and Yamamoto, T.T. (2004). The very low-density lipoprotein (VLDL) receptor: characterization

and functions as a peripheral lipoprotein receptor. J. Atherosclerosis Thromb. *11*, 200–208. https://doi.org/10.5551/jat.11.200.
25. Shin, K.C., Huh, J.Y., Ji, Y., Han, J.S., Han, S.M., Park, J., Nahmgoong, H., Lee, W.T., Jeon, Y.G., Kim, B., et al. (2022). VLDL-VLDLR axis facilitates brown fat thermogenesis through replenishment of lipid fuels and PPARbeta/delta activation. Cell Rep. *41*, 111806. https://doi.org/10.1016/j.celrep.2022.111806.
26. Digby, J.E., Montague, C.T., Sewter, C.P., Sanders, L., Wilkison, W.O., O'Rahilly, S., and Prins, J.B. (1998). Thiazolidinedione exposure increases the expression of uncoupling protein 1 in cultured human preadipocytes. Diabetes *47*, 138–141. https://doi.org/10.2337/diab.47.1.138.
27. Chouchani, E.T., Kazak, L., and Spiegelman, B.M. (2019). New Advances in Adaptive Thermogenesis: UCP1 and Beyond. Cell Metabol. *29*, 27–37. https://doi.org/10.1016/j.cmet.2018.11.002.
28. Boss, O., Samec, S., Paoloni-Giacobino, A., Rossier, C., Dulloo, A., Seydoux, J., Muzzin, P., and Giacobino, J.P. (1997). Uncoupling protein-3: a new member of the mitochondrial carrier family with tissue-specific expression. FEBS Lett. *408*, 39–42. https://doi.org/10.1016/s0014-5793(97)00384-0.
29. Krauss, S., Zhang, C.Y., and Lowell, B.B. (2005). The mitochondrial uncoupling-protein homologues. Nat. Rev. Mol. Cell Biol. *6*, 248–261. https://doi.org/10.1038/nrm1592.
30. Weisberg, S.P., McCann, D., Desai, M., Rosenbaum, M., Leibel, R.L., and Ferrante, A.W., Jr. (2003). Obesity is associated with macrophage accumulation in adipose tissue. J. Clin. Invest. *112*, 1796–1808. https://doi.org/10.1172/JCI19246.
31. Wen, J., and Wang, L. (2022). Identification of key genes and their association with immune infiltration in adipose tissue of obese patients: a bioinformatic analysis. Adipocyte *11*, 401–412. https://doi.org/10.1080/21623945.2022.2104512.
32. Wernstedt Asterholm, I., Tao, C., Morley, T.S., Wang, Q.A., Delgado-Lopez, F., Wang, Z.V., and Scherer, P.E. (2014). Adipocyte inflammation is essential for healthy adipose tissue expansion and remodeling. Cell Metabol. *20*, 103–118. https://doi.org/10.1016/j.cmet.2014.05.005.
33. Zhu, Z., Guo, L., Yeltai, N., Xu, H., and Zhang, Y. (2022). Chemokine (C-C motif) ligand 2-enhanced adipogenesis and angiogenesis of human adipose-derived stem cell and human umbilical vein endothelial cell co-culture system in adipose tissue engineering. J. Tissue Eng. Regen. Med. *16*, 163–176. https://doi.org/10.1002/term.3264.
34. Pappireddi, N., Martin, L., and Wühr, M. (2019). A Review on Quantitative Multiplexed Proteomics. Chembiochem *20*, 1210–1224. https://doi.org/10.1002/cbic.201800650.
35. Liu, D., Yang, S., Kavdia, K., Sifford, J.M., Wu, Z., Xie, B., Wang, Z., Pagala, V.R., Wang, H., Yu, K., et al. (2021). Deep Profiling of Microgram-Scale Proteome by Tandem Mass Tag Mass Spectrometry. J. Proteome Res. *20*, 337–345. https://doi.org/10.1021/acs.jproteome.0c00426.
36. Kim, S.C., and Wang, X. (2020). Phosphatidic acid: an emerging versatile class of cellular mediators. Essays Biochem. *64*, 533–546. https://doi.org/10.1042/EBC20190089.
37. Sankella, S., Garg, A., Horton, J.D., and Agarwal, A.K. (2014). Hepatic gluconeogenesis is enhanced by phosphatidic acid which remains uninhibited by insulin in lipodystrophic Agpat2-/- mice. J. Biol. Chem. *289*, 4762–4777. https://doi.org/10.1074/jbc.M113.530998.
38. Kastner, D.L., Aksentijevich, I., and Goldbach-Mansky, R. (2010). Autoinflammatory disease reloaded: a clinical perspective. Cell *140*, 784–790. https://doi.org/10.1016/j.cell.2010.03.002.
39. Kayser, B.D., Lhomme, M., Prifti, E., Da Cunha, C., Marquet, F., Chain, F., Naas, I., Pelloux, V., Dao, M.C., Kontush, A., et al. (2019). Phosphatidylglycerols are induced by gut dysbiosis and inflammation, and favorably modulate adipose tissue remodeling in obesity. Faseb. J. *33*, 4741–4754. https://doi.org/10.1096/fj.201801897R.
40. Santagostino, S.F., Assenmacher, C.A., Tarrant, J.C., Adedeji, A.O., and Radaelli, E. (2021). Mechanisms of Regulated Cell Death: Current Perspectives. Vet. Pathol. *58*, 596–623. https://doi.org/10.1177/03009858211005537.
41. Kist, M., and Vucic, D. (2021). Cell death pathways: intricate connections and disease implications. EMBO J. *40*, e106700. https://doi.org/10.15252/embj.2020106700.
42. Liang, D., Minikes, A.M., and Jiang, X. (2022). Ferroptosis at the intersection of lipid metabolism and cellular signaling. Mol. Cell *82*, 2215–2227. https://doi.org/10.1016/j.molcel.2022.03.022.
43. Driskell, R.R., Jahoda, C.A.B., Chuong, C.M., Watt, F.M., and Horsley, V. (2014). Defining dermal adipose tissue. Exp. Dermatol. *23*, 629–631. https://doi.org/10.1111/exd.12450.
44. Liu, S.Y., Wu, J.J., Chen, Z.H., Zou, M.L., Teng, Y.Y., Zhang, K.W., Li, Y.Y., Guo, D.Y., Yuan, F.L., and Li, X. (2022). Insight into the role of dermal white adipose tissue loss in dermal fibrosis. J. Cell. Physiol. *237*, 169–177. https://doi.org/10.1002/jcp.30552.
45. Angueira, A.R., Sakers, A.P., Holman, C.D., Cheng, L., Arbocco, M.N., Shamsi, F., Lynes, M.D., Shrestha, R., Okada, C., Batmanov, K., et al. (2021). Defining the lineage of thermogenic perivascular adipose tissue. Nat. Metab. *3*, 469–484. https://doi.org/10.1038/s42255-021-00380-0.
46. Forman, B.M., Tontonoz, P., Chen, J., Brun, R.P., Spiegelman, B.M., and Evans, R.M. (1995). 15-Deoxy-delta 12, 14-prostaglandin J2 is a ligand for the adipocyte determination factor PPAR gamma. Cell *83*, 803–812. https://doi.org/10.1016/0092-8674(95)90193-0.
47. Puhl, A.C., Milton, F.A., Cvoro, A., Sieglaff, D.H., Campos, J.C.L., Bernardes, A., Filgueira, C.S., Lindemann, J.L., Deng, T., Neves, F.A.R., et al. (2015). Mechanisms of peroxisome proliferator activated receptor gamma regulation by non-steroidal anti-inflammatory drugs. Nucl. Recept. Signal. *13*, e004. https://doi.org/10.1621/nrs.13004.
48. Wang, J., Wang, B., and Zhang, Y. (2020). Agonism activities of lyso-phosphatidylcholines (LPC) Ligands binding to peroxisome proliferator-activated receptor gamma (PPARgamma). J. Biomol. Struct. Dyn. *38*, 398–409. https://doi.org/10.1080/07391102.2019.1577175.
49. Lange, M., Angelidou, G., Ni, Z., Criscuolo, A., Schiller, J., Blüher, M., and Fedorova, M. (2021). AdipoAtlas: A reference lipidome for human white adipose tissue. Cell Rep. Med. *2*, 100407. https://doi.org/10.1016/j.xcrm.2021.100407.
50. Hajra, A.K., Larkins, L.K., Das, A.K., Hemati, N., Erickson, R.L., and MacDougald, O.A. (2000). Induction of the peroxisomal glycerolipid-synthesizing enzymes during differentiation of 3T3-L1 adipocytes. Role in triacylglycerol synthesis. J. Biol. Chem. *275*, 9441–9446.
51. Lodhi, I.J., and Semenkovich, C.F. (2014). Peroxisomes: a nexus for lipid metabolism and cellular signaling. Cell Metabol. *19*, 380–392. https://doi.org/10.1016/j.cmet.2014.01.002.
52. Dean, J.M., and Lodhi, I.J. (2018). Structural and functional roles of ether lipids. Protein Cell *9*, 196–206. https://doi.org/10.1007/s13238-017-0423-5.
53. Festa, E., Fretz, J., Berry, R., Schmidt, B., Rodeheffer, M., Horowitz, M., and Horsley, V. (2011). Adipocyte lineage cells contribute to the skin stem cell niche to drive hair cycling. Cell *146*, 761–771. https://doi.org/10.1016/j.cell.2011.07.019.
54. Nicu, C., Pople, J., Bonsell, L., Bhogal, R., Ansell, D.M., and Paus, R. (2018). A guide to studying human dermal adipocytes in situ. Exp. Dermatol. *27*, 589–602. https://doi.org/10.1111/exd.13549.
55. Rivera-Gonzalez, G., Shook, B., and Horsley, V. (2014). Adipocytes in skin health and disease. Cold Spring Harb. Perspect. Med. *4*, a015271. https://doi.org/10.1101/cshperspect.a015271.
56. Szczepanik-Kułak, P., Michalak-Stoma, A., and Krasowska, D. (2022). Usefulness of Dermoscopy in Localized Scleroderma (LoS, Morphea) Diagnosis and Assessment-Monocentric Cross-Sectional Study. J. Clin. Med. *11*, 764. https://doi.org/10.3390/jcm11030764.
57. Wang, Q.A., Tao, C., Gupta, R.K., and Scherer, P.E. (2013). Tracking adipogenesis during white adipose tissue development, expansion and regeneration. Nat. Med. *19*, 1338–1344. https://doi.org/10.1038/nm.3324.

CellPress
OPEN ACCESS

STAR★METHODS

KEY RESOURCES TABLE

REAGENT or RESOURCE	SOURCE	IDENTIFIER
Antibodies		
AGPAT2	Genway Biotech (custom made)	PMID: 21873652
Biological samples		
Adipose tissue depots	This study	N/A
Chemicals, peptides, and recombinant proteins		
RNA Stat-60	Fisher Scientific	Cat# nc9489785
cOmplete mini protease inhibitor tablets	Roche	Cat# 11836153001
Insulin	Sigma	Cat# I1882
IBMX	Sigma	Cat# I5879
Dexamethasone	Sigma	Cat# D1756
Rosiglitazone	Cayman Chemical	Cat# 71740
Indomethacin	Sigma	Cat# I8280
MCDB 201	Sigma	Cat# M6770
DMEM (low-glucose)	Life Technologies	Cat# 11885-084
ITS premix	Fisher Scientific	Cat# 41-400-045
L-ascorbic acid-2-2phosphate	Sigma	Cat# A8960
Mouse FGF-2	R&D Systems	Cat# 3139-FB-025/CF
Gentamicin	Fisher Scientific	Cat# 15-750-060
Antibiotic/Antimycotic	Life Technologies	Cat# 15240-062
DMEM/F12	Life Technologies	Cat# 11885-084
Oil Red O	Sigma	Cat# O625
Sybr Green	Thermo Fisher	Cat# 4364346
Collagenase D	Roche	Cat# 11088858001
BSA	Sigma	Cat# A3803
Fetal Bovine Serum	Sigma	Cat# 12303C
Doxycycline	Sigma	Cat# D3447
SPLASH Lipidomix standards	Avanti	Cat# 330707-1EA
Critical commercial assays		
RNeasy lipid mini extraction kit	Qiagen	Cat# 74804
DC Protein Assay Reagents Package	Bio-Rad	Cat# 5000116
Triglyceride Colorimetric Assay Kit	Cayman Chemical	Cat# 10010303
DNA-free™ DNA Removal Kit	Fisher Scientific	Cat# am1906
Reverse Transcription Reagents kit	Fisher Scientific	Cat# N8080234
DeadEnd™ Fluorometric System	Promega	Cat# G3250
Mouse Leptin ELISA Kit	Crystall Chem	Cat# 90030
TMT10plex Isobaric Mass Tagging Kit	Thermo Scientific	Cat# 90113
Pierce High pH Reversed-Phase Peptide Fractionation Kit	Thermo Scientific	Cat # 84868
Experimental models: Cell lines		
Primary adipose stromal vascular cells	This paper	N/A

(*Continued on next page*)

Continued

REAGENT or RESOURCE	SOURCE	IDENTIFIER
Experimental models: Organisms/strains		
Mouse: Agpat2$^{-/-}$	In house	PMID 19187773
Mouse: rtTA-adiponectin	In house	PMID 22451920
Mouse: Tg-AT-hA2; mA2$^{-/-}$	This paper	N/A
Oligonucleotides		
A full list of qPCR primers, see Table S1	This paper	N/A
Primer manufacturer	Integrated DNA Technologies	Coralville, IA
Primer manufacturer	Realtimeprimer.com	Elkin Park, PA
Recombinant DNA		
pBluescript-TRE-Tight	In house	PMID 22451920
Software and algorithms		
GraphPad Prism version 9.2.0	GraphPad Software	https://www.graphpad.com
FIJI (ImageJ version 1.52p)	NIH	https://fiji.sc/
BZ-X Analyzer version 1.4.1.1	Keyence	https://www.keyence.com/landing/microscope/lp_fluorescence.jsp
SAS version 9.4	SAS institute	https://www.sas.com
MultiQuant™	Sciex	https://sciex.com/products/software/multiquant-software
Proteome Discoverer v.3.0 SP1	Thermo Scientific	https://www.thermofisher.com
Other		
Doxycycline diet	Bio-Serv	Cat# S4107
Normal chow diet	Envigo	Cat# 2916
12 well collagen I coated plates (Biocoat)	Fisher Scientific	Cat# 08-774-2
60 mm collagen I Biocoat plate	Fisher Scientific	Cat# 08-774-7
10 cm collagen I Biocoat plate	Fisher Scientific	Cat# 08-772-75
Keyence BZ-X710 (Microscope for imaging)	Keyence	https://www.keyence.com
16 × 100 mm glass tubes with PTFE-lined caps	Fisher Scientific	Cat# 14-962-26F
Solvent-resistant plasticware pipette tips	Mettler-Toledo	Cat#30389164
2.0 mL prefilled Bead Ruptor tube (2.8 mm ceramic beads)	Omni International	19–628
SCIEX QTRAP 6500+	SCIEX	https://sciex.com/products/mass-spectrometers/qtrap-systems/qtrap-6500plus-system
Shimadzu LC-30AD HPLC system	Shimadzu	https://ssi.shimadzu.com/products/liquid-chromatography/index.html
150 × 2.1 mm, 5 μm Supelco Ascentis silica column	Supelco	Cat# 581509-U
Zirconium oxide beads 1.0 mm diameter	Next Advance	Cat # ZrOB10
Bruker Minispec mq10 (NMR)	Bruker Corporation	Billerica, MA
StepOne Plus Real-Time PCR System	Thermo Fisher Scientific	Waltham, MA
Bead Ruptor	Omni International	Kennesaw, GA

RESOURCE AVAILABILITY

Lead contact

Further information and requests for resources and reagents should be directed to and will be fulfilled by the lead contact, Anil Agarwal (anil.agarwal@utsouthwestern.edu).

Materials availability

Unique materials and reagents generated in this study are available upon request from the lead contact with a completed Material Transfer Agreement.

Data and code availability

- All data reported in this paper will be shared by the lead contact upon request.
- This paper does not report original code.
- Any additional information required to reanalyze the data reported in this paper is available from the lead contact upon request.

EXPERIMENTAL MODEL DETAILS

Mouse littermates of the same sex were randomly assigned to experimental groups. All animal studies were approved by the Institutional Use and Care of Animals Committee (IUCAC) at the University of Texas Southwestern Medical Center. All methods were performed in accordance with the relevant guidelines and regulations. All animals were kept in 12-h light/dark cycles at 22°C temperature. Mice were fed either standard chow diet or doxycycline diet, as indicated in the text.

Primary stromal vascular fraction (SVF) cells were derived from both male and female Tg-$^{AT\text{-}hA2}$;m*A2*$^{+/+}$ (WT) and Tg-$^{AT\text{-}hA2}$;m*A2*$^{-/-}$ mouse lines generated in this study. Cells were propagated in growth media and induced with differentiation media at 37°C as described in the STAR methods.

METHOD DETAILS

Generation of transgenic AGPAT2 mouse model

To generate Tg-TRE-h*AGPAT2*, the human *AGPAT2* open reading frame (GenBank: NM_006412) was amplified with the following primers, including a Kozak sequence on the forward primer and XbaI restriction sites (underlined) on both primers for ease of cloning: Forward – 5′ GCTCTAGAGCCGCCACCATGGAGCTGTGGCCGTG and Reverse – 5′ GCTCTAGATCTACTGGGCCGGCTGCAC. The amplified product was cloned into pDrive, then digested with XbaI to release the fragment. The fragment was then cloned in XbaI restricted pBluescript-TRE-Tight vector and h*AGPAT2* was Sanger sequenced to verify no PCR error occurred.

The strategy of linearizing this plasmid for injection with the recommended NaeI and SacII restriction sites was unusable because both sites are present in our h*AGPAT2* sequence. To overcome this difficulty, we designed primers to span the NaeI and SacII restriction sites of pBluescript-TRE-Tight-h*AGPAT2*, which were flanked by SpeI restriction sites (underlined). SpeI restriction sites are not present in the h*AGPAT2* sequence. Forward – 5′ GGACTAGTAGGGAAGAAAGCGAAAGGAG; Reverse – 5′ GGACTAGTCTAAAGGGAACAAAAGCTGGA.

This strategy will amplify an approximately 3 kb fragment containing h*AGPAT2*, as well as the promoter and rabbit β-hemoglobin 3′ UTR sequence from the pBluescript-TRE-Tight vector (Figure S1C).

The fragment was digested with SpeI and ligated into the same site into a vector of convenience for Sanger sequencing and amplification. Once the correct sequence was confirmed, the fragment was excised using SpeI, purified, and provided to the transgenic core. The linearized plasmid was microinjected into C57BL/6J fertilized eggs. The 8 male F0 mice were crossed with female C57BL/6J mice to confirm the transmission of the transgene. From these matings, a total of 42 pups were obtained from 8 litters. The F1 pup tail genomic DNA was examined by qPCR to determine the relative copy number of the h*AGPAT2* transgene, which varied from C_t 18.6 to 28.0. (Note: in qPCR, lower C_t values correspond to a higher gene expression). We randomly selected 6 males for further mating.

Since we wanted to express hAGPAT2 only in adipose tissue, we crossed 6 male Tg-TRE-h*AGPAT2* mice with the Tg-*Adipo*-rtTA mouse line (obtained from P.E. Scherer's lab). The cross between these two lines produced a mouse strain expressing both h*AGPAT2* and rtTA protein (Tg-h*AGPAT2*, *Adipo*-rtTA). This mouse line, when fed doxycycline, will activate the expression of *AGPAT2* in adipose tissue.

To determine that these mice express h*AGPAT2*, we crossed six mice and their progeny were genotyped for the presence of h*AGPAT2* and *rtTA*. Those mice that were positive for both transgenes were fed doxycycline (600 mg/kg) when they were 5–6 weeks old; the pellets were changed every alternate day for 2 weeks. Animals were euthanized at the end of 2 weeks and all three adipose tissues (brown, gonadal and subcutaneous) were collected. Total RNA was isolated and amplified for h*AGPAT2* by RT-qPCR. Raw C_t values for the expression of h*AGPAT2* were as follows: brown adipose tissue (BAT) C_t ~20–27, male gonadal adipose tissue C_t 21–25, subcutaneous adipose tissue (SubQ) C_t ~28–29. In our hands, the expression of h*AGPAT2* in both males and females was highest in BAT, followed by gonadal adipose tissue and lowest in SubQ. We also amplified endogenous mouse *Agpat2* to correlate the expression of h*AGPAT2* in these mice. Generally, the expression of h*AGPAT2* was slightly less than endogenous m*Agpat2*.

The expression of hAGPAT2 protein was further confirmed by immunoblot (Figure S1D). It is to be noted that the antibody raised against human AGPAT2 does not recognize mouse AGPAT2 protein (in-house experience). The immunoblot shows the presence of expressed human AGPAT2 in BAT and gonadal adipose tissue.

Generation of h*AGPAT2* expression in m*Agpat2*$^{-/-}$ background

Upon confirming the expression of h*AGPAT2* regulated by doxycycline, the L1 Tg-h*AGPAT2*, *Adipo*-rtTA mice were crossed with m*Agpat2*$^{+/-}$ mice to generate Tg-h*AGPAT2*, *Adipo*-rtTA, m*Agpat2*$^{+/-}$ mice. While genomic qPCR shows this line as having a lower copy number

integration, we proceeded with the L1 line because it had a good hAGPAT2 protein expression in adipose tissue. The Tg-h*AGPAT2*, *Adipo*-rtTA, m*Agpat2*$^{+/-}$ mice were genotyped and these Tg-h*AGPAT2*, *Adipo*-rtTA, m*Agpat2*$^{+/-}$ heterozygous mice were crossed to generate Tg-h*AGPAT2*, *Adipo*-rtTA, m*Agpat2*$^{-/-}$ mice. Tg-h*AGPAT2*, *Adipo*-rtTA, m*Agpat2*$^{-/-}$ mice were used for subsequent experiments. The mating strategy to obtain experimental animals is shown in Figure S1E. This mouse strain is abbreviated hereafter as **Tg-$^{AT\text{-}hA2}$;m*A2*$^{-/-}$**

Mouse genotyping

For genotyping of **Tg-$^{AT\text{-}hA2}$;m*A2*$^{-/-}$** mice, we used primers to amplify the Tg-TRE-h*AGPAT2*, Tg-*Adipo*-rtTA, and m*Agpat2* alleles individually: Tg-TRE-h*AGPAT2*: forward 5′ – ATGGAGCTGTGGCCGTGTCT – 3′, reverse 5′ – AGTACTTGAAGCTTCGCACG – 3′, with a product size of 217 bp. Tg-*Adipo*-rtTA: Forward 5′ – GAACAACGCCAAGTCATTCCGCTG – 3′, reverse 5′ – CTCCTGTTCCTCCAATACGCAGCC – 3′ with a product size of 212 bp. Both the amplification products were confirmed by Sanger sequencing. *Agpat2*$^{-/-}$ mice used in this study have been described.[7] Mice were genotyped using the following allele discriminating primer sets: A15, CGG CTA GGT AAG CAG TTT GA; A8, AAA GCT GTG CCA GGG TGG GT; and S175, GAT TGG GAA GAC AAT AGC AGG CAT GC. Genomic DNA amplified with A15 + A8 will produce the WT allele of 733 bp and A8+S175 will produce the knockout allele of 614 bp.

Magnetic resonance imaging and spectrometry

The whole body ^{1}H NMR spectra were collected on a Varian 4.7T horizontal image scanner using a ^{13}C-^{1}H linear coil (Varian, diameter 63 mm, length 115 mm). The fat contents were analyzed as the integral of the 1.3 ppm signal relative to the total integral of both 4.7 ppm signal (water) and the 1.3 ppm signal. T1-weighted images were collected on the same machine using either a ^{1}H Litz coil (Dorty, diameter 40 mm, length 50 mm) for axial images or a ^{13}C-^{1}H linear coil (Varian, diameter 63 mm, length 115 mm) for axial, sagittal, and coronal images. The MRI parameters were TR = 580 ms, TE = 12 ms, resolution 0.078 × 0.078 × 3 mm (axial) or 0.136 × 0.136 × 3 mm (coronal and sagittal). These images were obtained using 1.5 Tesla magnet and the animals were killed by cervical dislocation and all images were acquired within 30 min.

Nuclear magnetic resonance

Nuclear Magnetic Resonance (NMR) measurements of mice were obtained on the Bruker Minispec using the default parameters.

Differentiation of stromal vascular fraction (SVF) cells

The mice were anesthetized and SubQ and BAT fat pads were collected under sterile conditions and placed into 60 mm petri dishes with sterile PBS. The tissue was blotted dry on sterile gauze and transferred to 1 mL digest media [10 mL stock digest media (final concentrations: 100 mM HEPES pH 7.4, 120 mM NaCl, 50 mM KCl, 5 mM glucose, 1 mM $CaCl_2$), 10 mg collagenase D, 0.15 g BSA, per fat pad] in a new Petri dish. The tissue was finely minced with dissection scissors and transferred to a new 50 mL conical tube and the remaining 9 mL digest media was added. Tissues were digested at 37°C with shaking for 2 h. Tubes were vortexed on medium-high speed for a few seconds to facilitate dispersion of cells. Cells were filtered through 100 μm cell strainers into new 50 mL conical tubes to remove large debris and mature adipocytes. 30 mL PBS +2% FBS was added to each tube to rinse and cells were centrifuged at 600 x g for 5 min at 4°C. The upper adipocyte layer was aspirated and pelleted cells were resuspended in 10 mL PBS +2% FBS. Cells were filtered through a 40 μm cell strainer into a new 50 mL conical tube and 30 mL fresh PBS +2% FBS was added to wash. Cells were centrifuged at 600 x g for 5 min at 4°C and resuspended in 5 mL SVF media (DMEM/F12 containing Glutamax, sodium pyruvate, 2.438 g/L sodium bicarbonate, 10% FBS, 1% Abx/AM - 10,000 units/mL of penicillin, 10,000 μg/mL of streptomycin, and 25 μg/mL of Fungizone, 0.1% Gentamycin) and plated in a 6 cm collagen I coated dish. The media was changed the following day to remove red blood cells and debris. Cells were cultured until they reached 60–70% confluency and then transferred to a 10 cm collagen I coated dish. Cells were allowed to reach 100% confluency and then plated into 12-well collagen I coated plates. Cells were allowed to reach 100% confluency (very packed) and then induction was started (this was considered Day 0). The induction cocktail consisted of final concentrations of 1 μM Dexamethasone, 0.2 mM IBMX, 3 μM Indomethacin, 10 μg/mL Insulin and 1 μM Rosiglitazone in SVF media, and in some experiments **Tg-$^{AT\text{-}hA2}$;m*A2*$^{-/-}$** SVF cells received doxycycline at a final concentration of 1 μg/mL. The media was changed every other day to maintenance media which consisted of 10 μg/mL Insulin, 1 μM Rosiglitazone for all induced cells, with 1 μg/mL doxycycline for some **Tg-$^{AT\text{-}hA2}$;m*A2*$^{-/-}$** cells in SVF media. On day 8, one set of cells were fixed with 4% paraformaldehyde at room temperature for 20 min and then stained with Oil Red O (ORO) at room temperature for 10 min in the dark. ORO was removed simultaneously with the addition of PBS to prevent the cells drying out. 500 μL RNA Stat-60 was added to a second set of plates and RNA was isolated. Note, we also attempted SVF cell differentiation obtained from gonadal adipose tissue of both sexes, but could not obtain reproducible results.

Total RNA isolation

Total RNA was extracted from mouse adipose tissues (~50–100 mg) using RNA STAT-60. Total RNA from adipose tissue depots was extracted using RNeasy Lipid Tissue Kit according to the manufacture's protocol. RT-qPCR was carried out and analyzed as described below.

Reverse transcription quantitative polymerase chain reaction (RT-qPCR)

Total RNA, in equal quantity, was pooled from 2 to 6 samples of adipose tissue of each genotype and sex, and RT-qPCR was carried out in a 20 μL reaction volume. A total of 1–20 μg RNA was DNase I treated using the DNase-free kit from Ambion. Complementary DNA was made

using 1–2 μg DNase I-treated RNA using reverse-transcription kit from ABI. RT-qPCR was performed in duplicate using 2.5 mM primers, 20 ng complementary DNA, and SYBR Green. All RT-qPCR were carried out in 96-well plates using the StepOnePlus real-time PCR system. RT-qPCR was performed twice for liver samples and once for adipose tissue samples and in duplicate, and the transcript levels were normalized to *cyclophilin (cyclo)*. The ΔC_t value for each sample was calculated as ΔC_t = [C_t (gene of interest)-C_t (*cyclo*)]. The $\Delta\Delta C_t$ value for each gene of interest was calculated as $\Delta\Delta C_t$ = [ΔC_t (sample of interest) - ΔC_t (WT)]. The fold change was calculated as fold change = $2^{-\Delta\Delta Ct}$. Primers used for gene amplification were obtained from Harvard primer bank or were designed in-house and synthesized by Integrated DNA Technologies, or were obtained from realtimeprimers.com. Primers used in this study are provided in Table S1.

Quantitative PCR using pooled sample strategy

In a preliminary study, we amplified the expression of mRNA for several genes individually and in pooled samples and compared the raw C_t values for each gene. There is excellent correlation between the mean of individual samples to those when the samples are pooled. We now routinely pool the samples for measurements of mRNA expression. Furthermore, in the current study, in order to account for the experimental variance, we generated cDNA from the pooled samples two different times and amplified independently in duplicates.

Triacylglycerol (TAG) assay

Adipose tissue triacylglycerol (TAG) was measured using a triglyceride colorimetric assay kit from Cayman chemical according to the manufacturer's protocol with a few minor adjustments. A known quantity of 25–50 mg adipose tissue was weighed and homogenized in 1 mL of the buffer with protease inhibitor. The tissue homogenate was first spun at 3000 x g for 10 min at 4°C to break the excessive froth and transferred to a microfuge tube and spun again at 10,000 x g for 10 min. The supernatant was transferred to another tube, including the fat layer, and the volume noted. A preliminary dilution of the samples allowed us to determine the dilution appropriate to be within the range of the standard. The TAG is expressed as mg/g tissue.

TUNEL assay

To assess cell death, subcutaneous, gonadal, and brown adipose tissues were obtained from both male and female dox-fed Tg-$^{AT\text{-}hA2}$;*mA2*$^{-/-}$ mice. At 12 weeks, the doxycycline food was withdrawn and regular chow diet was provided for an additional 4 weeks, at which time the tissues were harvested from anesthetized mice following fixation via transcardial perfusion with 4% paraformaldehyde. Tg-$^{AT\text{-}hA2}$;*mA2*$^{-/-}$ mice used as controls continued to receive dox food the entire time. Subsequent paraffin processing, embedding and sectioning were performed by standard procedure. Terminal deoxynucleotidyltransferase-mediated UTP end label (TUNEL) staining for apoptotic cells was done according to the protocol supplied with Promega DeadEnd Fluorometric TUNEL System. Apoptotic cells were labeled with fluorescein, and the sections were counterstained with propidium iodide. Stained slides were imaged at 20x magnification (Keyence BZ-×710, software BZ -X viewer) at both ~470 nm (FITC) and 535 nm (Cy-3) fluorescent excitation and the red/green overlay in separate images and 9–17 fields per tissue were obtained. The obtained images were processed in FIJI (ImageJ) to count the number of nuclei (red), TUNEL positive (green), and colocalized cells. To achieve this, the images were adjusted to 8-bit, the default threshold was used with a dark background. Particles were analyzed with a circularity of 0.00–1.00 showing the outlines. The minimum pixel size was set to 10 pixels. The number of particles was counted by FIJI in separate red, green and colocalized drawings. The number of colocalized particles was divided by the number of nuclei (red particles) to obtain the percent of TUNEL positive cells. The percent TUNEL positive cells were averaged over all the obtained fields.

Lipid mass spectrometry

All solvents used were either HPLC or LC/MS grade and purchased from Sigma-Aldrich. Splash Lipidomix standards were purchased from Avanti. All lipid extractions were performed in 16 × 100 mm glass tubes with PTFE-lined caps. Glass Pasteur pipettes and solvent-resistant plasticware pipette tips were used to minimize leaching of polymers and plasticizers.

Approximately 25–50 mg of adipose tissue (gonadal fat, subcutaneous (SubQ), and brown adipose tissue) was transferred to a 2.0 mL prefilled Bead Ruptor tube, and 1 mL of methanol-dichloromethane (1:2; v/v) was added. The tissues were homogenized with a Bead Ruptor. The tissue homogenates were transferred to glass tubes and diluted to a final concentration of 20 mg/mL using the same solvent as above. Aliquots equivalent to 0.250 mg of homogenized tissue were transferred to fresh glass tubes for liquid-liquid extraction. Samples were extracted using a modified method of Bligh/Dyer; 3 mL of dichloromethane, methanol, and water (1:1:1 v/v/v) were added along with the sample. The mixture was vortexed and centrifuged at 2,671 x g for 5 min, resulting in two distinct liquid phases. The organic phase (lower phase) was drawn up with a Pasteur pipette and placed in a fresh glass tube and spiked with 20 μL of a 1:5 diluted S PLASH Lipidomix standard mixture. The samples were dried under liquid nitrogen and resuspended in 400 μL of hexane. Lipids were analyzed by LC-MS/MS using an SCIEX QTRAP 6500+ equipped with a Shimadzu LC-30AD high-performance liquid chromatography (HPLC) system and a 150 × 2.1 mm, 5 μm Supelco Ascentis silica column. Samples were injected at a flow rate of 0.3 mL/min at 2.5% solvent B (methyl *tert*-butyl ether) and 97.5% Solvent A (hexane). Solvent B was increased to 5% over 3 min and then to 60% over 6 min. Solvent B was subsequently decreased to 0% during 30 s while Solvent C, isopropanol-water (90:10 v/v) was set at 20% and increased to 40% during the following 11 min. Solvent C is increased to 44% over 6 min and then increased to 60% over 50 s. The system was held at 60% solvent C for 1 min prior to re-equilibration at 2.5% of solvent B for 5 min at a 1.2 mL/min flow rate. Solvent D [acetonitrile-water 95:5 (v/v) with 10 mM Ammonium acetate] was infused post-column at 0.03 mL/min. Column

oven temperature was 25°C. Data was acquired in positive and negative ionization mode using multiple reaction monitoring (MRM). The LC-MS/MS data was analyzed using MultiQuant software. The identified lipid species were normalized to its corresponding internal standard.

Tandem mass tag-mass spectrometry (TMT-MS) for adipose tissue

Sample preparation

Approximately 40–70 mg adipose tissues (SubQ, gonadal and brown) were dispensed in snap cap 2 mL tubes with 400 μl of RIPA buffer (minus the Triton X-100) containing protease inhibitor cocktail. Approximately 150 mg of beads were added to each tube of Zirconium oxide beads and homogenized using Bullet Blender according to the manufacturer's suggested protocol for adipose tissue (Next Advance). The homogenates were centrifuged at 10,000 x g for 10 min at 4°C and the layer below the fat layer was transferred to another tube. The lysates were centrifuged again at the same speed and time and supernatant was saved in a clean tube to avoid any residual fat. The volume of tissue lysates were measured and appropriate quantity of 25% Triton X-100 was added to final concentration of 1%. The lysates were kept on ice for ~45–60 min and sonicated 3 × 5 s at 35% amplitude using Sonics Vibracell with cooling, protein was measured with the DC assay kit and lysate was used for TMT mass spectrometry as follows.

Peptide labeling and fractionation

SDS was added to the tissue samples in RIPA buffer to bring it to a starting concentration of 3–5% SDS in 50 μL. Tris(2-carboxyethyl)phosphine (TCEP) was added to a final concentration of 20 mM and samples were incubated at 56°C for 30 min. After cooling, iodoacetamide was added to a final concentration of 20 mM and samples were incubated for 30 min at room temperature in the dark. 50 μg samples were then transferred to S-Trap micro columns and digested overnight with 2 μg of trypsin at 37°C. Following digestion, the peptide eluate was dried and reconstituted in 100 mM TEAB buffer. The TMT10plex Isobaric Mass Tagging Kit was used to label the peptides, as per the manufacturer's instructions. The labeled reactions were cleaned and fractionated using Pierce High pH Reversed-Phase Peptide Fractionation Kit into 8 fractions according to the manufacturer's directions. The fractions were dried in a SpeedVac and reconstituted in a 2% acetonitrile, 0.1% TFA buffer.

Peptides mass spectrometry

Peptides were analyzed on a Thermo Orbitrap Eclipse MS system coupled to an Ultimate 3000 RSLC-Nano liquid chromatography system. Samples were injected onto a 75 μm i.d., 75-cm long EasySpray column and eluted with a gradient from 0 to 28% buffer B over 180 min at a flow rate of 250 nL/min. Buffer A contained 2% (v/v) ACN and 0.1% formic acid in water, and buffer B contained 80% (v/v) ACN (acetonitrile), 10% (v/v) trifluoroethanol, and 0.1% formic acid in water at a flow rate of 250 nL/min. Spectra were continuously acquired in a data-dependent manner throughout the gradient, acquiring a full scan in the Orbitrap [at 120,000 resolution with a standard AGC (automatic gain control) target] followed by MS/MS scans on the most abundant ions in 2.5 s in the ion trap (turbo scan type with an intensity threshold of 5,000, CID (collisionally induced dissociation) collision energy of 35%, standard AGC target, maximum injection time of 35 m and isolation width of 0.7 m/z). Charge states from 2 to 6 were included. Dynamic exclusion was enabled with a repeat count of 1, an exclusion duration of 25 s and an exclusion mass width of ±10 ppm. Real-time search was used for selection of peaks for SPS-MS3 (synchronous precursor selection-mass spectrometry to the thrid-MS3) analysis, with searches performed against the mouse reviewed protein database from UniProt along with the sequence of human AGPAT2. Up to 1 missed tryptic cleavage was allowed, with carbamidomethylation (+57.0215) of cysteine and TMT reagent (+229.1629) of lysine and peptide N-termini used as static modifications and oxidation (+15.9949) of methionine used as a variable modification. MS3 data were collected for up to 10 MS2 peaks that matched to fragments from the real-time peptide search identification, in the orbitrap at a resolution of 50,000, HCD (high-energy C-trap dissociation) collision energy of 65% and a scan range of 100–500 m/z, which allows a sufficient range of reporter ions to be detected.

Protein identification

Protein identification and quantification were done using Proteome Discoverer v.3.0 SP1. Raw MS data files were analyzed against the mouse reviewed protein database from UniProt along with the sequence of human AGPAT2. Both Comet and Sequest HT with INFERYS Rescoring were used, with carbamidomethylation (+57.0215) of cysteine and TMT reagent (+229.1629) of lysine and peptide N-termini used as static modifications and oxidation (+15.9949) of methionine used as a variable modification. Reporter ion intensities were reported, with further normalization performed by using the total intensity in each channel to correct discrepancies in sample amount in each channel. The false-discovery rate (FDR) cutoff was 1% for all peptides. Extracted reporter ions were further normalized by using total intensity in each channel to correct sample amount error.

Histological analysis

Adipose tissue from 12 to 24-week-old mice were fixed in 4% paraformaldehyde 48 h, embedded in paraffin, sectioned, and stained with hematoxylin and eosin (H&E).

Dorsal and inguinal skin was excised from 12 weeks male and female mice. The skin was excised from the mouse, taking care to remove the subcutaneous layer along with the skin. The skin was attached to a piece of cardboard to prevent the curling of the edges and fixed for 48 h in 4% paraformaldehyde. The skin was washed with PBS and incubated in a 10% sucrose solution in PBS for 12 h at 4°C. The solution was

changed to 18% sucrose in PBS. The samples were cryosectioned and stained with Oil Red O (ORO) and counter stained with H&E. Dorsal skin was excised from 24 weeks male and female mice. The skin was excised from the mouse, taking care to remove the subcutaneous layer along with the skin. The skin was fixed for 48 h in 4% paraformaldehyde in a cassette between 2 pieces of foam to avoid curling of the edges. The skin was then embedded in paraffin, sectioned, and stained with H&E. All images were acquired with a Keyence BZ-X710 microscope. The black balance was adjusted in BZ-X analyzer software, version 1.3.0.3. Adipocyte size and number was determined using the BZ-X analyzer software. All tissues were processed at the pathology core laboratory at the University of Texas Southwestern Medical Center in Dallas, Texas.

Plasma leptin measurements

Plasma leptin was measured by ELISA method as per the manufacture's suggestion.

QUANTIFICATION AND STATISTICAL ANALYSIS

No statistical methods were used to predetermine sample size. No method of randomization was used to determine how mice were allocated to experimental groups. The statistical method used for each dataset is indicated for each figure in the figure legend. Statistical tests used are Student's *t* test, two-way ANOVA, mixed model repeated measurements, Wilcoxon rank-sum test, and one-way ANOVA. We determined the sex interaction for each experimental dataset to ascertain if the male and female data could be combined, which could improve the statistical power/effect. On occasion, we did observe a sex interaction, but not in all experimental datasets. Since there was no consistency in the sex interaction, we are presenting the male and female data separately. All analyses were performed using SAS 9.4. Statistical tests are two-sided, and $p < 0.05$ is considered as significant. $^{*}p < 0.05$, $^{**}p < 0.001$, $^{***}p < 0.0001$. Data are presented as mean $\pm$ SD.